Characterization of the interaction between protein loaded polymeric nanoparticles and supported lipid bilayers towards improved drug delivery systems

Caractérisation de l'interaction entre nanoparticules polymériques chargées de protéines et bicouches lipidiques sur support solide en vue d'une amélioration des traitements médicamenteux

Laura DE BATTICE
Division of Biological physics
Department of Applied Physics
CHALMERS UNIVERSITY OF TECHNOLOGY
Göteborg, Sweden, 2010

In collaboration with the UNIVERSITY OF LIEGE (Belgium)
Supervisors: Sofia SVEDHEM (Chalmers University of Technology, Sweden)
Christian GRANDFILS (University of Liège, Belgium)
Examinors (Chalmers): Sofia Svedhem
Examining committee (ULg): Christian Grandfils
Nicolas Paquot
Vincent Seutin
Vincent Geenen

Abstract

The development of nanoparticles (NPs) for the delivery of therapeutic agents has introduced new opportunities for the improvement of medical treatment. Among these opportunities, surface based analytical techniques are promising tools to improve our understanding of biointerfacial phenomena, such as NP interactions at biological barriers. The University of Liège (ULg), Belgium, has recently developed electrostatically assembled NPs, made of polycationic polymers and biopharmaceutical drugs with the intention of promoting their delivery through non-invasive administration. Adopting polymers of four different number average molecular weight (Mn) and procedures of the ULg, we successfully reproduced the preparation of those NPs either loaded with Human Insulin (HI) or chicken Ovalbumin (OVA). The formulation of this latter protein has highlighted interesting findings related to problems in its solubilization. An unexpected aggregation of this protein has been directly correlated to the agitation mode adopted and was found to be time and pH dependent. NPs, prepared at Chalmers or provided by the ULg, were characterised by Dynamic Light Scattering (DLS) and Nanoparticle Tracking Analysis (NTA). Typically, NP size was about 200 nm in diameter with a relatively good agreement between these two techniques. In addition, the analysis of their electrophoretic mobility (zeta potential measurement) showed that these NPs were positively charged with a zeta potential of around +25 mV. Difficulties were encountered with respect to the OVA dissolution state, and high-quality OVA loaded NPs could not be formed. This interesting aggregation phenomenon, that could not be totally suppressed, was found to depend on pH, on filtering, and on time of dissolution. Using the Quartz Crystal Microbalance with Dissipation monitoring technique (QCM-D), we studied in real time the interaction between HI loaded NPs and both neutral and negatively charged model lipid membranes, successfully formed on SiO_2 coated crystals. First, the four polycationic polymers of different Mn were investigated. We found that the electrostatic properties of the polymers had a determinant role in their interaction with the model lipid membranes: on a negatively charged model lipid membrane, the polycations irrespectively of their Mn collapsed and formed thin and rigid layers, whereas hydrated viscoelastic layers, as indicated by a high dissipation by QCM-D, were formed on a neutral membrane. A different behaviour was observed for the NPs. We found that, on a negatively charged membrane, NPs formed increasingly dissipative layers for higher Mn of the polycation used to prepare the NPs. Thicker layers were formed on a neutral membrane. Functionalized NPs with a ternary compound were also investigated. Interestingly, without modifying drastically the mean size or the Zeta potential of the NP, the presence of this additional compound was shown to alter completely the adsorption profile and total amount of NP on the negatively charged membrane, with appearance of a transient mass uptake. The difference in interaction profiles between binary and ternary NPs makes the study of those NPs very interesting in terms of drug release.

Abrégé

Le développement des nanoparticules (NPs) pour l'administration aux patients d'agents thérapeutiques nous offre de nouvelles possibilités d'améliorer les soins médicaux. Parmi ces possibilités, les techniques analytiques basées sur l'étude des surfaces sont des outils prometteurs pour une meilleure compréhension des phénomènes biointerfaciaux, tels que les interactions des NPs au niveau des barrières biologiques. L'Université de Liège (ULg), Belgique, a récemment développé des NPs assemblées électrostatiquement et constituées de polymères polycationiques et de médicaments biopharmaceutiques en vue de promouvoir leur administration aux patients par des voies non-invasives. En choisissant des polymères de quatre Mn (poids moléculaire moyen) différents et en adoptant les procédures de l'ULg, nous avons réussi à reproduire la préparation de ces NPs chargées, soit d'insuline humaine (HI), soit d'Ovalbumine (OVA) de poulet. La préparation de cette dernière a mis en lumière d'intéressantes constatations concernant des problèmes de solubilisation. Nous ne nous étions pas attendus à une agrégation de cette protéine. Nous l'avons immédiatement mise en relation avec le mode d'agitation utilisé et elle s'est révélée dépendante du temps et du pH. Les NPs, tant celles préparées par nous, que celles fournies par l'ULg, furent caractérisées par les techniques appelées Dynamic Light Scattering (DLS) et Nanoparticle Tracking Analysis (NTA). Typiquement, la taille des NPs était d'environ 200 nm de diamètre avec une concordance relativement bonne entre les deux techniques utilisées. De plus, l'analyse de la mobilité électrophorétique (zeta potential measurement) des NPs a révélé qu'elles étaient chargées positivement d'un potentiel Zeta évalué à environ +25mV. Des difficultés sont apparues dans l'état de dissolution de l'OVA, et nous n'avons pas pu former de NPs chargées d'OVA qui soient de bonne qualité. Cet intéressant phénomène d'agrégation, qui n'a pas pu être totalement éliminé, s'est montré dépendant du pH, de la filtration, et de la durée de dissolution. En utilisant la technique de la microbalance à cristaux de quartz avec contrôle de dissipation (QCM-D), nous avons étudié en temps réel l'interaction entre des NPs chargées d'Insuline Humaine (HI) et des modèles de membranes lipidiques, dont la charge était soit neutre, soit négative, et qui se sont formées avec succès sur des cristaux recouverts de SiO_2. Nous avons d'abord soumis à l'examen les quatre polymères polycationiques de différents Mn et nous avons constaté que les propriétés électrostatiques des polymères jouaient un rôle déterminant dans leur interaction avec les membranes lipidiques modèles : sur une membrane chargée négativement, les polycations, quel que soit leur Mn, s'effondraient et formaient des couches fines et rigides, tandis que des couches viscoélastiques hydratées, comme l'indique une dissipation élevée détectée par QCM-D, se formaient sur membrane neutre. Nous avons observé un comportement différent chez les NPs. Sur une membrane chargée négativement, elles formaient des couches dont la dissipation croissait avec un Mn plus élevé du polycation utilisé pour préparer les NPs. Sur une membrane neutre, les NPs formaient des couches épaisses et hydratées. L'ULg nous a également fourni des NPs contenant un composé ternaire. De manière tout à fait intéressante, sans modifier considérablement la taille moyenne et le potentiel Zeta de la

NP, la présence de ce composé supplémentaire s'est révélée modifiant complètement le profil d'adsorption et le nombre total de NPs sur la membrane chargée négativement, avec l'apparition d'un apport transitoire de masse. Les différences de profils d'interactions entre NPs binaires et ternaires peuvent se traduire par des différences dans les mécanismes d'assimilation des médicaments.

I Preface

This diploma thesis was done as part of the Erasmus program in collaboration between the department of Applied Physics of Chalmers University of Technology (Sweden) and the Research Centre of Biomaterials (CEIB) of the University of Liège (ULg), Belgium.

The project developed in it is part of a relatively new research area called nanobiotechnology, endeavoring to develop new ways for drug delivery in order to reduce the invasive nature of certain treatments, to improve selectivity, bioavailability, efficiency and cost of drug delivery systems.

Novel drug nanocarriers are being developed at the ULg and novel approaches to nanodrug characterization based on surface-sensitive analytical techniques are being developed at Chalmers University of Technology. This joint effort is carried out within the EU project called Nanoscale Functionalities for Targeted Delivery of Biopharmaceutics (NanoBioPharmaceutics).

II List of abbreviations

DLS	Dynamic Light Scattering
EIS	Electrochemical Impedance Spectroscopy
HI	Human Insulin
LDV	Laser Doppler Velocimetry
LYSO	LYSOzyme
Mn	Number average Molecular weight
Mw	Molecular weight
NP	NanoParticle
NTA	Nanoparticle Tracking Analysis
OVA	OVAlbumin
PBS	Phosphate Buffered Saline
PdI	Polydispersity Index
PEC	PolyElectrolyte Complex
pI	Isoelectric point
POPC	1-Palmitoyl-2-Oleoyl-sn-glycero-3-PhosphoCholine
POPS	1-Palmitoyl-2-Oleoyl-sn-glycero-3-[Phospho-L-Serine]
QCM-D	Quartz Crystal Microbalance with Dissipation monitoring
SDS	Sodium Dodecyl Sulfate
SLB	Supported Lipid Bilayer
Tris	Tris(hydroxymethyl)aminomethane
ZP	Zeta Potential

III Table of contents

IV Introduction

Research on nanoscale biosystems constitutes very dynamic domain in science and technology at the confluence of physical sciences, molecular engineering, biology, biotechnology, and medicine. Medicine is constantly evolving owing to new technologies. Among them, nano-sized drug carriers are announced to improve 21st century's health care by providing significant potential advantages. In this work we studied some nanodrug carriers loaded with Human Insulin (HI) as a potential treatment for diabetes disease. This section provides an overview of the medical context of diabetes and a discussion of the roles of NPs in the drug delivery research area. It introduces the model system used, and the aims and strategy adopted in this work.

IV.1 Medical context of diabetes

Diabetes is a chronic disease characterized by hyperglycemia that is responsible for 6.8% of the overall death rate assessed in the world among the 20-79-year-old.[1]

Whether it is of type I or of type II, if it is not treated or not properly treated, diabetes on the long run causes neuropathy, retinopathy, cardiovascular diseases, peripheral vascular diseases, and cerebrovascular accidents.[2] To prevent those complications, a glycemic control must be set up.[3] It consists in mimicking the physiological secretion of insulin with the administration of this hormone, in order to reach a glycated hemoglobin (HbA1c) rate lower than 7%, according to the American Diabetes Association (ADA). [4-5] The HbA1c rate measures the proportion in blood of hemoglobin molecules to which glucose has attached.

In 1922 Banting and Best used animal-sourced insulin successfully for the first time in clinical medicine as a treatment for a 14-year-old boy suffering from type I diabetes.[6] Today a great variety of injectable solutions exists, ranging from rapid- and ultra-rapid-acting preparations to be used at meal time, to intermediate- and long-acting preparations designed to replace the physiological secretion of insulin.

Fig. 1
Syringes for insulin injection
(Disposable Syringes Co., Ltd)

However, the administration by subcutaneous injections remains a painful and invasive procedure sometimes difficult to implement on patients who often are

[1] Roglic and Unwin, *Mortality attributable to diabetes: Estimates for the year 2010*, Diabetes Research and Clinical Practice (2010) **87:** 15-19
[2] Nathan, *Long-term complications of diabetes-mellitus*, New England Journal of Medicine (1993) **328:** 1676-1685
[3] Shamoon *et al., The effect of intensive treatment of diabetes on the development and progression of long-term complications in insulin-dependent diabetes-mellitus.*, New England Journal of Medicine (1993) **329:** 977-986
[4] Lassmann-Vague and Raccah, *Alternatives routes of insulin delivery*, Diabetes & Metabolism (2006) **32:** 513-522
[5] Pham *et al., Inhaled human rDNA origin insulin, a novel formulation for diabetes mellitus*, Journal of Clinical Pharmacology (2007) **47:** 890-903
[6] Banting, F. *et al., Pancreatic extracts in the treatment of diabetes mellitus*, Canadian Medical Association Journal (1922) **12:** 141-146

reluctant to have daily injections. This way of administration therefore suffers from lack of patient compliance.[7]

That is why new strategies have been developed by scientists to set up alternative non-invasive ways of administering insulin by ocular, vaginal, rectal, transdermal, gastrointestinal, oral, nasal and pulmonary routes.[4]

Up to now, only the pulmonary delivery route of insulin has reached the medicine market in 2006 with Exubera®, a product distributed by Pfizer Company. This system, based on the inhalation of a dry powder, was designed for patients suffering from type I or type II diabetes.[4-7] However, in October 2007, Pfizer decided to withdraw this formulation from the market, in line with a negative risk-benefit balance.[8]

Other pulmonary systems were developed, in particular AERx® (Aradigm Corp, Hayward, CA, USA and NovoNordisk, Copenhagen, Denmark) which were based on HI spray cans. But today the clinical trials on AERx® have been interrupted too because of adverse events.[9]

A lot of work has still to be done in this line of research. One possible strategy takes advantage of "nano-carriers". These can be of diverse nature. They can be lipid-based, like liposomes, micelles, lipid-drug complexes and lipid emulsions. They can be polymer microspheres immunoconjugates, polymer drug conjugates etc.[10] Polymer drug conjugates, together with other more specific systems, constitute a relatively new research field that has a huge potential to improve drug delivery systems.

For example, polymeric nanoscaled molecules are extensively studied for their capacity to protect and target biopharmaceutical drugs such as peptides and proteins.

IV.2 Nanoparticles for drug delivery

NPs for drug delivery are part of a relatively new research field called nanobiotechnology. Their role is to minimize adverse systemic effects of medical treatments by protecting, targeting, and finally releasing a drug at a specific site in the body.[11] For that purpose, NPs are for example designed to interact with biological

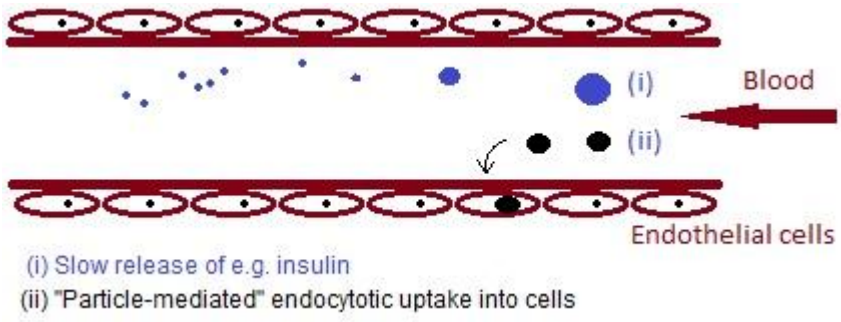

Fig. 2
Schematic drawing of a NP interacting through specific targeting with a model lipid membrane

[7] Galan, d. *et al.*, *Efficacy and safety of inhaled insulin in the treatment of diabetes mellitus*, Netherlands Journal of Medicine (2006) **64:** 319-325
[8] Mathieu and Gale, *Inhaled insulin: gone with the wind?*, Diabetologia (2008) **1:** 1-5
[9] Hermansen, K. *et al.*, *Intensive Therapy With Inhaled Insulin via the AERx Insulin Diabetes Management System*, Diabetes care (2004) **27:** 162-167
[10] Allen and Cullis, *Drug delivery systems: Entering the mainstream*, Science (2004) **303:** 1818-1822
[11] Li and Huang, *Pharmacokinetics and biodistribution of nanoparticles*, Molecular Pharmaceutics (2008) **5:** 496-504

interface through specific target-ligand interactions (see Fig. 2).

One of the major problems with drugs is their poor solubility in biological medium. This is an essential drawback for their effectiveness. Since nearly half of new chemical-based drugs are poorly soluble in water, the pharmaceutical companies are confronted with the big challenge of developing drugs with a higher surface/volume ratio that will increase their solubility. NPs appear to cope with this issue.[12]

As NP formulations improve absorption of insoluble compounds and macromolecules in the body, they enhance bioavailability and release rates, thereby allowing dose reduction and higher safety through reduced side effects.[12]

Direct coupling of drugs to targeting ligands is restricted to a few drug molecules. But the covalent link of a ligand to a drug carrier allows the combination of thousands of drug molecules by means of one receptor-targeted ligand.[13]

NPs make the reduction of administration frequency possible. They can be loaded with both hydrophilic and hydrophobic drugs and be involved in several routes of administration, like inhalation and oral ingestion. They are also highly stable and have a high carrier capacity.[14]

NPs are promising as delivery systems for DNA vaccines[15] and for the gene therapy field[12]. For example, apatite NPs are promising candidates for nonviral gene delivery. Poly(D,L-lactide-co-glycolide) NPs loaded with wt-p53 DNA have demonstrated a sustained antiproliferative effect in a breast cancer cell line[16]. Gelatin-based NPs have been reported to be safe and effective vectors for gene delivery in solid tumors. Clinical trials of the latter method are expected in the near future.[17]

NPs for drug delivery can be of diverse nature. There are for example polymeric NPs like polyelectrolyte complexes (PECs) and polymeric vesicles; there are liposomes, inorganic NPs, etc.

PECs form spontaneously when oppositely charged polyions are mixed, the drug commonly being the negatively charged ones. They are held together by electrostatic interactions (mainly), hydrogen bounding, hydrophobic interactions and van der Waals forces. Size distribution and charge of the PECs are dependent on concentration, ionic strength, pH, properties of the polymer used and way of mixing.

PECs are widely studied to improve drug delivery systems since ribonucleic acids and most proteins are negatively charged at physiological pH. Recently, more attention has been focused on using protein-

---

[12] Kewal and Jain, The Handbook of Nanomedicine, Humana Press, Totowa (2008) 165-167

[13] Vasir *et al.*, *Nanosystems in drug targeting: Opportunities and challenges*, Current Nanoscience (2005) **1:** 47-64

[14] Gelperina *et al.*, *The potential advantages of nanoparticle drug delivery systems in chemotherapy of tuberculosis*, American Journal of Respiratory and Critical Care Medicine (2005) **172:** 1487-1490

[15] Cui and Mumper, *Microparticles and nanoparticles as delivery systems for DNA vaccines*, Critical Reviews in Therapeutic Drug Carrier Systems (2003) **20:** 103-137

[16] Prabha and Labhasetwar, *Nanoparticle-mediated wild-type p53 gene delivery results in sustained antiproliferative activity in breast cancer cells*, Molecular Pharmaceutics (2004) **1:** 211-219

[17] Kommareddy and Amiji, *Antiangiogenic gene therapy with systemically administered sFlt-1 plasmid DNA in engineered gelatin-based nanovectors*, Cancer Gene Therapy (2007) **14:** 488-498

based-PECs to improve drug delivery systems.[18-19] Polymers commonly used in those systems can be biopolymers, such as chitosan, or synthetic polymers, such as poly(amido amines)s (PAAs).

The NPs used in this work are PECs consisting of electrostatically assembled polycationic polymers (polycations) and a proteinaceous drug (either HI or OVA).

Different parameters will be investigated in order to define the main features characterising the interaction between them and model lipid membranes, such as the importance of electrostatic interaction and the influence of Mn of the polycation used to make the NPs. The study of the interaction between PECs and model lipid membranes will be performed using Quartz Crystal Microbalance with Dissipation monitoring (QCM-D). Other techniques, like Atomic Force Microscopy and Surface Plasmon Resonance are also suitable for that kind of study.

IV.3 Biological barriers

Drug formulations differ depending on the desired administration route. Whatever administering way (oral, vaginal, rectal, transdermal, gastrointestinal, pulmonary, nasal or ocular) is chosen, NPs designed for drug delivery have to pass biological barriers in order to reach their target cells. The oral way is mostly preferred for its simplicity and often for economic reasons. Drugs administered that way can be produced in large amounts on an industrial scale and in a great variety of formulation (liquid (suspension, emulsion, linctuses), solid (tablets, capsules), etc.) dealt out in small and large doses (up to 1g of active ingredient in one tablet).

The drug formulation will first be confronted with gastric acidity (pH 1 to 3.5) during its transit through the stomach (from 5 min to 12 h), where it is also exposed to digestive enzymes (gastric lipase, etc.). It must then pass the pylorus, where most of the absorption takes place. And eventually the non-absorbed remains are eliminated in the feces. The active ingredients — first freed from their excipient, then dissolved — will have to pass the digestive tract membranes to reach the blood circulation.

To pass the biological barriers, NPs have a substantial advantage: they are small. So they can be transported through the cells by endocytosis, or in between cells by paracellular transport, or by carrier-mediated transport for

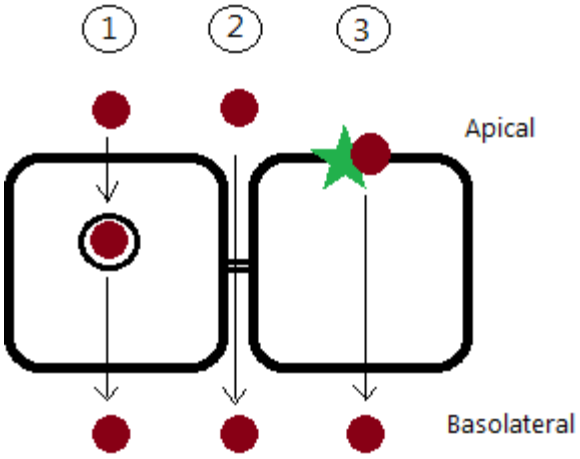

Fig. 3
Schematic drawing showing the possible drug transport mechanisms across mucosal epithelium: endocytosis-transcytosis-pinocytosis (1), paracellular transport (2), carrier-mediated transport (3)

[18] A. Harada, K. Kataoka, Novel polyion complex micelles entrapping enzyme molecules in the core : Preparation of narrowly distributed micelles from lysozyme and poly(ethylene glycol)-poly(aspartic acid)block copolymer in aqueous medium. Macromolecules, 31 (1998) 288-294.
[19] M. Mahkam, Starch-based polymeric carriers for oral insulin delivery, Journal of Biomedical Material Research Part A. 92A (2010) 1392-1397.

molecules smaller than 500 Da, as depicted in Fig. 3.

Several physiological factors influence the drug absorption. The two most important of them are (i) the digestive juice pH, which ranges from 1.5 in the gastric area to 8 in the intestine; (ii) the membrane absorbing surface available, which differs from area to area. This surface is particularly vast in the small intestine compared with the absorption surface of the stomach and the large intestine. Other factors play a role too, such as speed of both gastric emptying and intestinal transit. Two kinds of physico-chemical factors are relevant for gastro-intestinal absorption: those concerning the nature and characteristics of the active ingredients and those concerning the drug pharmaceutical form.

IV.4 How nanoparticles are taken up by the targeted cells

In order to develop more effective therapeutic agents, their accuracy in reaching the targeted cells must be enhanced. This requirement can be met by designing NPs in different ways according to the nature of three factors: the cell to be reached, the drug to be delivered, the therapeutic effect to be attained. Two different ways can be mentioned:

1) *Equipping the NPs for specific interaction NP/targeted cell*.

Example: For a drug exclusively aimed at a specific type of cell, NPs must be designed bearing a ligand that is specific to a receptor that can only be expressed on the surface of the target cells. So the NPs can stick to these cells and release their load of drug, which will then be absorbed by the target cells. [20] (see Fig. 4)

Fig. 4
Schematic drawing of specific interaction between a nanoparticle loaded with drug molecules, and a target cell, inducing drug uptake by the cell.

2) *Equipping the carrier NPs to enable them to keep their load of drugs* for systemic action, while passing the biological environments and barriers they encounter, until they reach the blood circulation
Example: NPs equipped that way are particularly well suited for proteinaceous drugs like insulin this project is about.

[20] Alexis F, Pridgen E, Molnar LK, Farokhzad OC. Factors affecting the clearance and biodistribution of polymeric nanoparticles. *Mol Pharm*. 2008;5(4):505–515

IV.5 Model Lipid Membranes – Definition

To characterize the interaction of NPs with biointerfaces, we used a biomimetic model lipid membrane prepared on a solid sensor surface. This lipid bilayer membrane is continuous and supported by an underlying substrate (generally made of SiO_2 or TiO_2). It is often referred to as "Supported Lipid Bilayer (SLB)". It is formed by exposing liposomes on a hydrophilic substrate. Phospholipids are generally used for liposome formation.

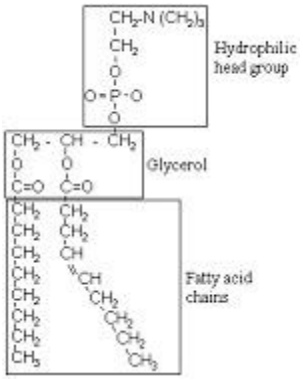

Fig. 5
Structure of a phospholipid. It is composed of one hydrophilic head group linked to two fatty acid chains by a glycerol groupment.

Due to their amphiphilic properties, when these molecules are placed in an aqueous medium, they organize themselves in such a way that their hydrophilic head groups face to water while their hydrophobic tails are insulated from the aqueous environment. Most phospholipids also have an additional chemical group bound to the phosphate. For example, they may be connected with choline; the resulting phospholipid is called phosphatidylcholine. SLBs are generated according to a three-step process, i.e.: (a) liposome deposition and adsorption to the substrate, (b) rupture and merging of liposomes to create lipid patches, (c) formation of a continuous SLB. In this study, we have adopted a membrane with a ~5nm thickness made of a phospholipid bilayer consisting of two layers of amphiphilic lipid molecules (see Fig. 6). SLBs formed on SiO_2 substrates generally maintain a 10Å thick layer of water between the membrane and the underlying substrate thus preserving many properties of free membranes.[21]

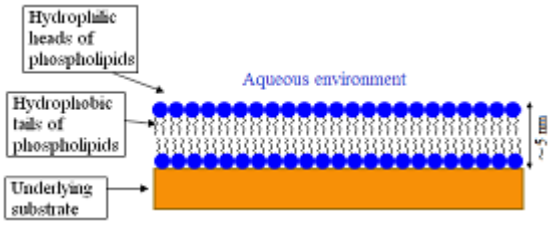

Fig. 6
Supported Lipid Bilayers are composed by 2 layers of phospholipids lying on a solid substrate.

SLBs are extensively used to study interfacial processes. For example they provide an excellent platform to study lipid transfer between them and adsorbing vesicles. This model is particularly relevant in order to better assess important biochemical processes including transmembrane transport, endo- and exocytosis, and function of membrane bound molecules.[22] SLBs are also used to study ligand–receptor binding processes, especially with respect to multivalent interactions.[23] In the immune cell recognition research area, SLBs offer useful model system allowing the exploration of basic features of molecular interactions in adhesive contacts between cells.[24]

SLBs are of great interest due to their simplicity of production, their mechanical stability and their applicability to many surface-sensitive analytical techniques such as atomic force microscopy, QCM-D,

---

[21] Gromelski *et al.*, *The formation of lipid bilayers on surfaces*, Colloids and Surfaces B-Biointerfaces (2009) **74:** 477-483
[22] Dimitrievski and Kasemo, *Simulations of lipid transfer between a supported lipid bilayer and adsorbing vesicles*, Colloids and Surfaces B-Biointerfaces (2010) **75:** 454-465
[23] Jung *et al.*, *Multivalent ligand-receptor binding on supported lipid bilayers*, J. Struct. Biol. (2009) **168:** 90-94
[24] Dustin, *Supported bilayers at the vanguard of immune cell activation studies*, J. Struct. Biol. (2009) **168:** 152-160

surface plasmon resonance and total internal reflection fluorescence microscopy.[25]

For example they are used to study

- the biological transduction with surface plasmon resonance[26],
- the role of polyunsaturated long fatty acids on membrane function with QCM-D[27],
- the kinetics of vesicle-to-bilayer transformation with both QCM-D and Surface Plasmon Resonance[28].

Note that SLBs are only a model for the study of interactions between NPs and lipid membranes. Thus, even if they have many advantages, they are not representative of what can happen in real biological situations. For example, no proteins are enclosed in the lipid bilayers, as opposed to real lipid cell membranes. Furthermore, even if a thin water film separates the bilayer from the substrate, the mobility of SLBs is much more limited. So, the next step after this kind of in vitro study is to test the NP formulation in vivo for a better understanding of the system in physiological situations.

Various other model systems of biological membrane can be used to mimic the cell surface environment. Among them, liposomes and bicelles are the most common.[29] Liposomes (also called lipid vesicles) are spherical particles consisting of a lipid bilayer entrapping an aqueous solution. They are used for a variety of applications. For example they are very well suited for transport studies since they define two aqueous phases separated by a lipid bilayer. They are also used for their capacity to entrap drug molecules, which makes them potential vehicles in drug delivery systems.[30] Bicelles are discoïdal lipid aggregates used for example for reconstitution of membrane proteins[31] or for crystallization of membrane proteins.[32-33]

IV.6 Polycations

Polycationic polymers, also called polycations, are extensively studied for their capacity to act as nanocarrier with a view to develop new drug delivery systems. Polycations can form polyelectrolytes complexes (PECs) with negatively charged molecules such as certain drugs (e.g. proteinaceous drugs), they appear to be of great interest to be used as drug carriers. For example, polycations have been

---

[25] Sundh M, S. S., Sutherland DS, *Influence of phase separating lipids on supported lipid bilayer formation at SiO2 surfaces*, Physical Chemistry Chemical Physics (2010) **2:** 453-460

[26] Heyse *et al.*, *Incorporation of rhodopsin in laterally structured supported membranes: observation of transducin activation with spatially and time-resolved surface plasmon resonance*, Biochemistry (1998) **2:** 507-522

[27] Dorota Thid, J. J. B., Sofia Svedhem, Bengt Kasemo, and Julie Gold, *DHA-Induced Changes of Supported Lipid Membrane Morphology*, Langmuir (2007) 5878-5881

[28] E. Reimuhlt, M. Z., F Höök, and B. Kasemo, *A Multitechnique Study of Liposome Adsorption on Au and Lipid Bilayer Formation on SiO_2*, Langmuir (2006) 3313-3319

[29] Corvera E, M. O., Singer MA, Zuckermann MJ, *The permeability and the effect of acyl-chain length for phospholipid bilayers containing cholesterol: theory and experiment*, Biochimica et Biophysica Acta (1992) **2:** 261-270

[30] Torchilin, *Recent advances with liposomes as pharmaceutical carriers*, Nature reviews. Drug discovery (2005) **2:** 145-160

[31] Czerski L, S. C., *Functionality of a membrane protein in bicelles*, Analytical Biochemistry (2000) **2:** 327-333

[32] Sanders CR, P. R., *Bicelles: a model membrane system for all seasons?*, Structure (1998) **10:** 1227-1234

[33] Faham S, B. J., *Bicelle crystallization: a new method for crystallizing membrane proteins yields a monomeric bacteriorhodopsin structure*, Journal of Molecular Biology (2002) **1:** 1-6

complexed with anti-inflammatory drugs[34]. As RNA and DNA are both negatively charged proteins, they have been extensively studied for their potential to be used in gene delivery systems when complexed with polycations[35].

Pr. Christian Grandfils, ULg, provided us with polycations of 4 different sizes studied for their potential usefulness as a new diabetes treatment when coupled to HI to form binary PECs. The Mn (Number average molecular weight) of the 4 polycations are the following:

- Polycation 1: Mn = 90,000 Da
- Polycation 2: Mn = 40,000 Da
- Polycation 3: Mn = 20,000 Da
- Polycation 4: Mn = 10,000 Da

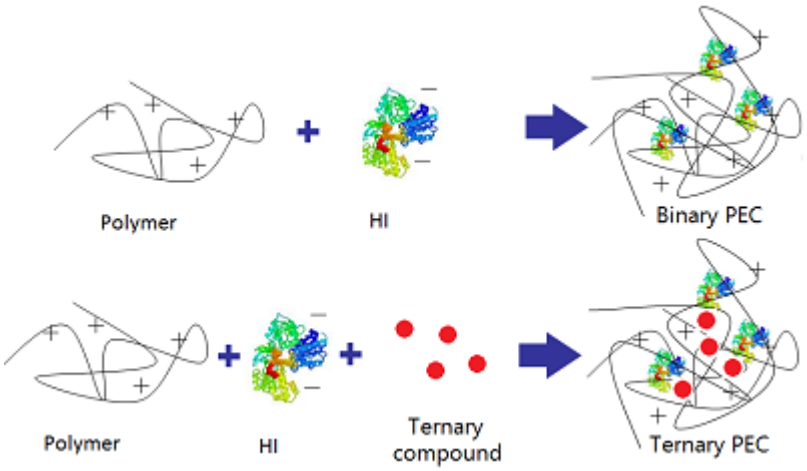

Fig. 7 Schematic illustration of the composition of binary and ternary PECs.

Polycations 1, 2, 3 and 4 form respectively binary PECs 1, 2, 3 and 4 when coupled to HI.

Christian Grandfils also provided us with a ternary compound that is assumed to improve the formulation stability of the NPs. We ended up with two sets of NPs, one set of binary PECs and one set of ternary PECs, that are illustrated in Fig. 7.

IV.7 Proteins

Lysozyme (LYSO) is a protein recognized by Alexander Fleming in 1922 as a bacteriolytic agent having an ability to hydrolyze bacterial cell walls. LYSO has a Mw (Molecular Weight) of approximately 14.7 kDa and an isoelectric point (pI) of around 11. In aqueous solution, this protein is a small monomer, compact and nearly spherical. These last 3 properties, combined with a relative stability and easy availability make LYSO an excellent choice for investigating the sensitivity of Dynamic Light Scattering (DLS) technique. [36-37-38-39]

Ovalbumin (OVA) is the major protein component in the hen egg, which consists of 54 % of egg

---

[34] Nandini and Cherng-ju, *Water-soluble polycations as oral drug carriers (tablets)*, Journal of Pharmaceutical Sciences (2000) **86:** 1339-1344

[35] Cho *et al.*, *Polycation gene delivery systems: escape from endosomes to cytosol.*, J Pharm Pharmacol (2003) **6:** 721-734

[36] Martinez-Fleites *et al.*, *The crystal structure of a family GH25 lysozyme from Bacillus anthracis implies a neighboring-group catalytic mechanism with retention of anomeric configuration*, Carbohydrate Research (2009) **344:** 1753-1757

[37] Ghalanbor *et al.*, *Improved Lysozyme Stability and Release Properties of Poly(lactide-co-glycolide) Implants Prepared by Hot-Melt Extrusion*, Pharm. Res. (2010) **27:** 371-379

[38] Blake *et al.*, *Structure of hen egg-white lysozyme - a 3 dimensional Fourier synthesis at 2A resolution*, Nature (1965) **206:** 757

[39] Li *et al.*, *Spectrophotometric studies on the binding of Vitamin C to lysozyme and bovine liver catalase*, Journal of Luminescence (2008) **128:** 1399-1406

white proteins. It is a globular protein with a Mw of 43 kDa and a pI of 4.6. [40-41] At neutral pH, it has therefore a net negative charge. This protein was first chosen as a model to form PECs. However, due to some problems concerning its dissolution state, more attention than expected had to be given to its preparation. OVA is a key ingredient in many food products because of its ability to form a three-dimensional network after denaturation by heat, that is, its ability to form gels in an irreversible way.[42-43] Gelation properties of OVA, such as viscosity, are affected by pH and concentration of protein and salt.

HI plays a key role in regulating the energy and glucose metabolism of our body. It is a peptidic hormone with a Mw of 5.8 kDa and a pI of 5.4.[44] Produced by the Langerhans islets of the pancreas, it triggers the absorption of blood glucose by liver, muscles and fat tissues and its future storage under the form of glycogen. Injection of HI is required in diabetes resulting from the body's failure to produce enough HI.

IV.8 Aim and plan

The aim of this thesis is to study the interaction between polymeric NPs loaded with proteins and model lipid membranes of different charges. To do so, several parameters will be investigated, such as the size of the polycation used to prepare the NPs and the presence or absence of a ternary compound, and several techniques will be used.

The planned chronological steps are the following:

- Preparation and characterization of protein and polycation solutions;
- Preparation and characterization of PEC solutions by complexing polycations and proteins, aiming at narrow size distributions;
- Establish relationship between polycation Mn and PEC size;
- Selection of high quality PEC solutions to be used for further experiments;
- Formation of good quality SLBs on SiO_2 coated quartz crystal sensors;
- Characterization of the interaction between PECs and SLBs using a surface sensitive analytical technique called QCM-D for different:

[40] Photchanachai *et al.*, *Heating of an ovalbumin solution at neutral pH and high temperature*, Bioscience Biotechnology and Biochemistry (2002) **66:** 1635-1640

[41] Gehrke *et al., Protein sorption and recovery by hydrogels using principles of aqueous two-phase extraction,* Biotechnology and Bioengineering (1998) **58:** 416-427

[42] Sanchez-Gimeno *et al., Studies of ovalbumin gelation in the presence of carrageenans and after manothermosonication treatments*, Innovative Food Science & Emerging Technologies (2006) **7:** 270-274

[43] Hatta *et al., Turbidity and hardness of a heat-induced gel of hen egg ovalbumin*, Agricultural and Biological Chemistry (1986) **50:** 2083-2089

[44] Wintersteiner and Abramson, *The isoelectric point of insulin,* Biol Chem (1932) 741-753

- SLB charges (ranging from negatively charged to neutral)
- PEC sizes

– Establish relationships between PEC properties and the nature of the interaction with SLBs with respect to the degree of reversibility of the process and to the structure of the adsorbed PECs.

Optional steps

– Compare the integrity of the membrane before and after adsorption of PEC solutions containing a ternary compound;

– Determine the degree of hydration of adsorbed PEC layers on one type of SLB.

V Experimental techniques

This section will introduce us to the techniques used in this thesis for:

– lipid vesicle extrusion,

– characterization of solutions (UV spectrophotometry, DLS, Zeta Potential measurements, and Nanoparticle Tracking Analysis (NTA)),

– surface based analytical study of NP-membrane interactions (QCM-D, Electrochemichal Impedance Spectroscopy and Reflectometry).

V.1 Lipid vesicle extrusion

Extrusion is one of the most common methods adopted to produce monodisperse lipid vesicles by forcing an aqueous suspension of lipid through polycarbonate membranes. For this work we used one of the extruders available on the market, the Avanti Polar Lipid Mini Extruder that is depicted on Fig. 8 and Fig. 9.

Fig. 8
Mini extruder from Avanti Polar Lipids used for lipid vesicles extrusion.

The most significant advantage of extrusion is that the resulting mean vesicle size and size distribution are reproducible from batch to batch. Moreover, extrusion is a mild technique that does not affect lipid structure.[45]

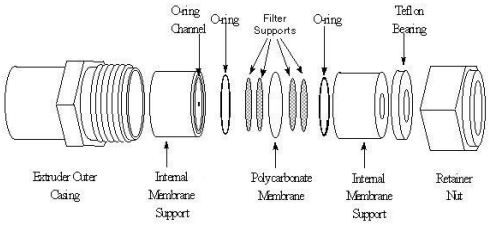

Fig. 9
Scheme of the mini extruder assembly from Avanti Polar Lipids.

A common alternative method to prepare lipid vesicles is sonication. With this method, lipid suspensions are treated using acoustic energy. The primary advantage of sonication over extrusion is that it is less time-consuming. However, the resulting vesicle batch-to-batch mean diameter and size distribution are not as reproducible as those provided by extrusion. Furthermore, contamination often occurs due to particles released from the sonication

[45] Lapinski *et al.*, *Comparison of liposomes formed by sonication and extrusion: Rotational and translational diffusion of an embedded chromophore*, Langmuir (2007) **23:** 11677-11683

probe/bath.[46]

V.2 UV spectrophotometry

UV spectrophotometry is a commonly used analytical technique to characterize biologically active substances. It measures the absorption of a monochromatic ultraviolet radiation by the active substances. The degree of absorption by a substance is proportional to its concentration according to the Beer-Lambert law (Eq. 1):

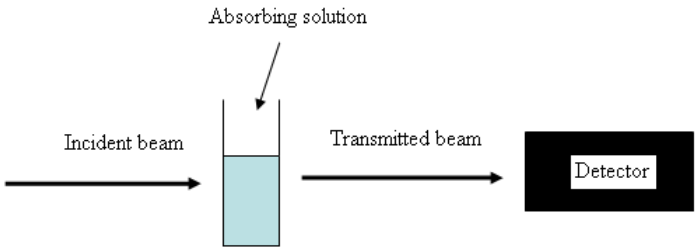

Fig. 10 Basic principle of UV spectrophotometry
An incident light beam is projected on an absorbing solution. The transmitted light beam reaches a detector. Incident and transmitted intensities are compared, giving information on characteristics of the solution.

Eq. 1 Beer-Lambert law

$$A = \log_{10}\left(\frac{I}{I_0}\right) = \varepsilon l C$$

A = Absorbance
I_0 = incident light beam Intensity
I = transmitted light beam Intensity
ε = coefficient of molar extinction
l = path length
C = concentration

Phenylalanine, tryptophane and tyrosine are 3 aromatic amino acids residues (see Fig. 11) that dominate protein UV spectra around 280 nm, they are called chromophore groups. Although the absorption maxima for certain proteins may be at other wavelengths, 280 nm is favored because proteins absorb strongly there while other substances commonly in protein solutions do not. Two very common applications of UV spectrophotometry are the identification of proteins, and the determination of their concentration in solutions.

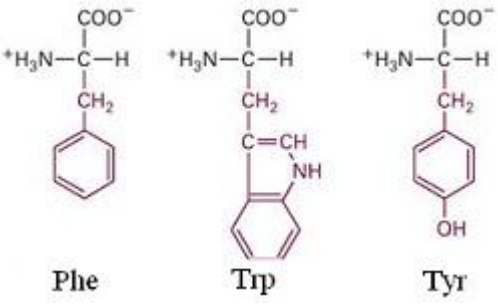

Fig. 11
Chemical structure of 3 aminoacids residues absorbing at 280 nm in UV spectrophotometry.

V.3 Dynamic Light Scattering

DLS is a technique used to determine the size distribution profile of particles ranging from a few nanometers to a few micrometers in suspension.

Particles suspended in a liquid are animated by a continuous motion, known as the Brownian motion. Due to their higher diffusion coefficients, small particles move quicker than bigger ones. This phenomenon is illustrated in Fig. 12, where the evolution of the respective positions of big and small particles in a liquid medium are schematized after a short interval of time, for instance 100 µs.

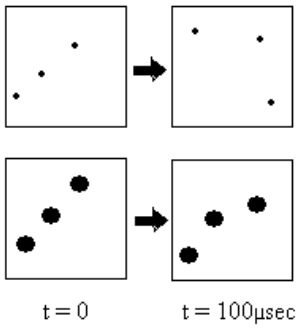

Fig. 12
Movement of big and small particles under Brownian motion

[46] Lapinski, Castro-Forero et al., *Comparison of liposomes formed by sonication and extrusion: Rotational and translational diffusion of an embedded chromophore*, Langmuir (2007) **23:** 11677-11683

In DLS, the suspension of particles is irradiated by a laser beam with a wavelength ranging typically from 488 to 633 nm. Light scattered by the particles is analysed as a function of time at a certain angle (often fixed at 90°). The time-variation in light scattering intensity, typically analysed with a resolution from 10 ns to several hundreds of ms, depends on the diffusion coefficient of particles (see Fig. 13) and therefore on their size. From the deconvolution of the correlation curve derived from this light scattering intensity fluctuation signal, the diffusion coefficient of the particles is mathematically derived. The Stokes-Einstein equation (Eq. 2)[47] is finally adopted in order to calculate the particle size (hydrodynamic radius) of the particles present in suspension:

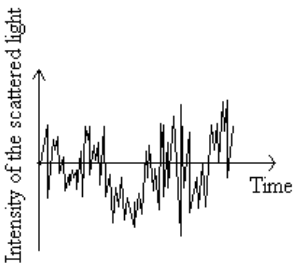

Fig. 13
Variation of the intensity of the scattered light in DLS

Eq. 2 Stokes-Einstein equation

$$R_h = \frac{k_B T}{6\pi\eta D}$$

r_h = Hydrodynamic Radius
k_B = Boltzmann constant
T = Temperature
η = Viscosity of the medium
D = Diffusion coefficient

The final particle size distribution can be determined from an average light intensity distribution. The resolution of polydisperse samples is difficult to handle due to the difficulty in realizing the deconvolution of the autocorrelation curves.

DLS is the preferred technique to determine the size of NPs, due to its simplicity of realization and its rapidity in data acquisition.[48-49] One of its main drawback (but in some case an advantage) is its high sensitivity to the presence of large particles.[50] This is due to the fact that the intensity of the scattered light is proportional to the 6th power of the particle diameter.[51] Therefore, dust or small amounts of large aggregates can significantly interfere with size determination of distinctly smaller size particles.[52]

[47] Malvern Instrument
[48] Filipe *et al.*, *Critical Evaluation of Nanoparticle Tracking Analysis (NTA) by NanoSight for the Measurement of Nanoparticles and Protein Aggregates*, Pharm. Res. (2010) **27:** 796-810
[49] Bootz *et al.*, *Comparison of scanning electron microscopy, dynamic light scattering and analytical ultracentrifugation for the sizing of poly(butyl cyanoacrylate) nanoparticles*, European Journal of Pharmaceutics and Biopharmaceutics (2004) **57:** 369-375
[50] Filipe, Hawe et al., *Critical Evaluation of Nanoparticle Tracking Analysis (NTA) by NanoSight for the Measurement of Nanoparticles and Protein Aggregates*, Pharm. Res. (2010) **27:** 796-810
[51] Demeester J, S. S., Sanders N, Haustraete J, *Methods for structural analysis of protein pharmaceuticals*, (2005)
[52] Berne B, P. R., *Dynamic light scattering with applications to chemistry, biology and physics*, (2000)

V.4 Zeta potential and zeta potential measurements

Electrokinetics potential, also called Zeta potential, is an important surface property of any colloidal systems which controls their stability. In a liquid, when particles bear electric charges at their surface (ionic groups, adsorbed ions, …), a gradient of ions is generated according to the so-called "Double-layer" model and as depicted on Fig. 14. This ion-gradient will determine the profile of the drop of electrochemical potential from the surface of the particle to the surrounding liquid. As a summary this double-layer consists of inner layer (called *stern layer*) where the ions are strongly bound to the surface of the particle owing to electrostatic interactions and an outer layer (called *diffuse layer*) where ions are loosely associated. The boundary between the liquid plane remaining cohesive to the particle in motion, introduced somewhere within the diffuse layer and the bulk liquid, is defined as the slipping plane. The ions and liquid linked to the inner layer will remain associated to the surface of the particles during their movement in the liquid and they will thereby control the electrokinetic potential of the particles. The potential at the slipping plane, called *Zeta potential* (ZP), is the difference of electrical voltage between this boundary and the liquid bulk. The magnitude of the ZP gives an indication the overall charge (measured at the slipping plane) that a particle acquires in a liquid. The magnitude of the ZP gives an indication of the stability of a colloidal system. If, within a solution, all particles are either positively charged or negatively charged with a large ZP, their repulsive electrostatic forces will stabilize the dispersion. On the other hand, if all particles have a low ZP, the repulsive electrostatic forces will not be strong enough to counteract attractive forces (e.g. Van der Waals) to prevent aggregation. As a general rule of thumb, the dividing line between stable and unstable dispersion is located at potentials of around |25-30| mV. Under these potential values the solution is generally considered unstable.[53]

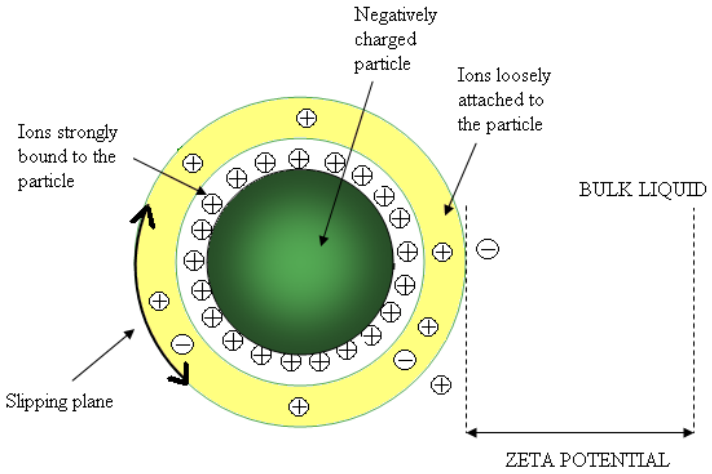

Fig. 14 Theoretical representation of Zeta Potential

ZP can be calculated from values obtained by *Laser Doppler Velocimetry (LDV)*. This technique measures the electrophoretic mobility (U_E) of charged particles in a solution subjected to an electric field. The particle suspension is injected in a capillary cell bordered at their two lateral ends by electrodes. When an electric field of a certain amplitude (E) is applied between them, charged particles move in direction of the electrode of opposite charge with an electrophoretic speed (V) which is calculated as

[53] Roland, Piel et al., *Systematic characterization of oil-in-water emulsions for formulation design*, International Journal of Pharmaceutics (2003) **263:** 85-94

follow:

Eq. 3

$$U_E = \frac{V}{E}$$

A visible laser beam (incident beam) is focused on the solution and scattered by the moving particles. This causes a shift in frequency (ΔF) because of the Doppler effect. The frequency of the scattered beam is then detected and compared with the frequency of a reference light beam. The higher the particles' speed, the bigger the frequency shift, the relation between them is expressed in the following equation:

Eq. 4

$$\Delta F = 2nV \sin(\frac{\vartheta/2}{\lambda_0})$$

Where n is the refractive index of the medium, V the particles' speed, λ_0 the wavelength of the incident light beam and θ the detection angle compared to the incident light beam. Knowing the magnitude of that frequency shift, one can determine the electrophoretic mobility of the particles.

Then, once the electrophoretic mobility is known, one can calculate the ZP value of the particles moving in the solution using the Henry equation (Eq. 5)[54]:

$$U_E = \frac{2\varepsilon z f(ka)}{3\eta}$$

Eq. 5 Henry equation

U_E = Electrophoretic mobility
ε = Dielectric constant
z = zeta potential
f(ka) = Henry's function
η = Viscosity

Where ε is the dielectric constant of the medium, z is the ZP, η is the viscosity of the medium and f(ka) is the Henry's function that equals 1.5 for particles in polar media and 1.0 for particles in non polar media.[55] As U_E has previously been calculated and as F(ka), η and ε are known values, the ZP value can be determined with this equation.

V.5 Nanoparticle Tracking Analysis

NTA is a technique for detection and analysis of NPs dispersed in a liquid medium. This technique relies also on the scattering of light of a visible laser beam. The set-up consists of a laser source, a liquid chamber and a microscope (see Fig. 15).

The particle suspension is injected in a viewing chamber where a laser light beam is focused. Scattered photons are detected individually thanks to an ultra-rapid and sensitive CCD camera. By tracking the particle movement, the rate of Brownian motion can be calculated. This rate is then related to

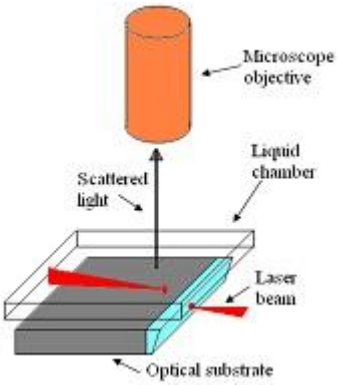

Fig. 15 NTA set-up

[54] Malvern Instrument, user manual
[55] Silver Colloids, official website

particle size according to the Stokes-Einstein equation (Eq. 2).[56] The NTA technique can detect particles as small as 10-20 nm depending on the nature of the solvent and of the particles. For the smallest size range (i.e. below 30 nm), only particles with a high difference in refractive index with liquid medium can be detected (e.g. gold or silver particles). The upper detection limit is around 1 μm, depending also on the nature of the solvent and on the particle type. An important application of the NTA technique is the characterization of polydisperse samples (i.e. heterogeneous in composition and/or containing a wide range of particle sizes).[57]

Using NTA, the lower size detection limit is defined by the particle size and the particle's refractive index. For particles having a very high refractive index such as colloidal gold, accurate determination of size can be achieved down to 10 nm in diameter. For lower refractive index particles, such as those of biological origin, the smallest detectable size might be between 25-35nm. Upper size limits are approached when the Brownian motion of a particle becomes too limited to track accurately, typically 1-2 μm diameter.[58] The lower detection limit of proteins and PECs is about 30 nm. For example, NTA is efficient to detect aggregation in protein solutions.[59]

V.6 Quartz Crystal Microbalance with Dissipation monitoring

QCM-D is a sensitive instrument that monitors in real time mass deposition (ng/cm²). The technique is based on the piezoelectric property of quartz allowing the conversion of a mechanical stimulation into an electric signal and vice versa. The fundamental theory behind QCM-D technique is explained in several articles[60-61-62] and theses[63-64].

---

[56] Nanosight, Ltd., Minton park, Amesbury, Wiltshire SP4 7RT, UK

[57] *Applications of Nanoparticle Tracking Analysis (NTA) in Nanoparticle Research*, http://www.schaefer-tec.com/fileadmin/user_upload/sortiment/nanopartikel/NanoSight/NANOSIGHT_Application_Review_NTA_April_2009_M2201B.pdf (accessed 2024/2005/2010)

[58] NANOSIGHT_Application_Review_NTA_April_2009_M201B.pdf accessed on the 27th of June, 2010

[59] Mahler *et al.*, *Protein Aggregation: Pathways, Induction Factors and Analysis*, Journal of Pharmaceutical Sciences (2009) **98:** 2909-2934

[60] Rodahl *et al.*, *Quartz crystal microbalance setup for frequency and Q factor measurements in gaseous and liquid environments*, Review of Scientific Instruments (1995) **7:** 3924-3930

[61] Hook *et al.*, *Energy dissipation kinetics for protein and antibody-antigen adsorption under shear oscillation on a quartz crystal microbalance*, Langmuir (1998) **14:** 729-734

[62] Irwin *et al.*, *Analysis of interpenetrating polymer networks via quartz crystal microbalance with dissipation monitoring*, Langmuir (2005) **21:** 5529-5536

[63] Ohlsson, *Miniaturized cell and flow reactor for QCM-D measurements on fluids and soft matter*, Chalmers University of Technology (2009)

[64] Edvardsson, *QCM-D with focus on variations in oscillation amplitude*, Chalmers University of Technology (2006)

V.6.1 Fundamental principles of Quartz Crystal Microbalance

The piezoelectricity phenomenon allows to couple the electrical and mechanical properties of a material. When a piezoelectric material is submitted to a mechanical force, it generates an electric field (piezoelectric effect). Inversely, if exposed to an electric field, it lengthens or shortens according to the polarity of the field, and in proportion to the strength of the field (inverse piezoelectric effect). This behaviour originates from the fact that piezoelectric materials, like quartz, possess a crystalline structure in which subdomains have opposite electrostatic net charges.

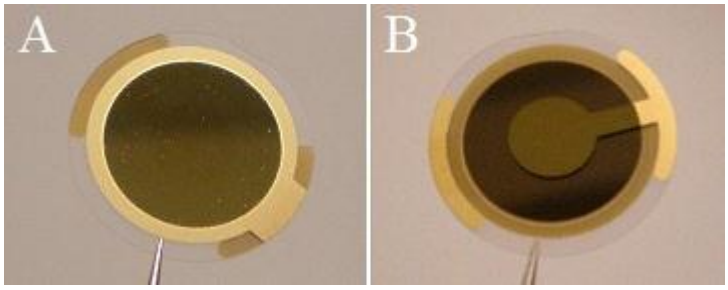

Fig. 16
Top (A) and bottom (B) faces of a standard commercial gold-coated quartz crystal used for QCM-D measurements.

Fig. 17
Shear motion of a quartz crystal

When an electromagnetic field is applied to the material, the domains will orient themselves, causing a strain in the crystal structure. The main part of the QCM-D instrument consists of an AT cut quartz crystal plate covered with metal electrodes deposited on both faces by evaporation (see Fig. 16). AT cut indicates a specific angle at which the quartz crystal is cut (a Y cut rotated 35°15' to the optic axis) and which has proven to be particularly suitable for an applied voltage to induce a suitable thickness shear wave (see Fig. 17). Under an alternating voltage, the strain amplitude of the stimulated quartz crystal will oscillate with the same frequency than the stimulating voltage.

The oscillation amplitude of the quartz crystal ranges from one to a few Å. At a certain frequency, called the resonance frequency, the oscillation of the quartz crystal has a harmonic behaviour with a maximum amplitude and a low energy loss. This frequency, called the fundamental resonance frequency, is 4.95 MHz for an AT cut quartz crystal having a thickness of 300 µm. The oscillation amplitude of the quartz crystal at different overtones follows a Gaussian distribution over the quartz crystal surface (see Fig. 18). Note that the amplitude maximum is in the middle of the sensor surface, that part of the crystal is therefore the most sensitive.

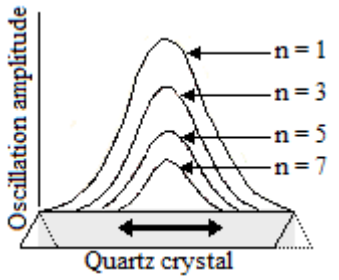

Fig. 18
The oscillation amplitude of the quartz follows a Gaussian distribution. Higher overtones have lower amplitudes and smaller widths.

The fundamental principle of the QCM sensing is the following: any mass added or removed from the crystal surface induces a shift in the resonance frequency of the crystal (ΔF) proportional to the mass

change on the crystal surface in accordance with the Sauerbrey equation (Eq. 6)[65]:

Eq. 6

$$\Delta m = \frac{C}{n}\Delta f$$

Δm = Mass change (=$m_{acoustic}$)
C = Mass sensitivity constant
n = Overtone number (1, 3, 5, 7…)
Δf = Frequency shift

This phenomenon is illustrated in Fig. 19, showing a decrease in the resonance frequency when a mass is adsorbed on the crystal.

The mass sensitivity constant depends on the thickness of the quartz plate and on the intrinsic properties of the quartz. C = -17.7 ng Hz^{-1} cm^{-2} in liquid phase for a resonance frequency of 4.95 MHz. The Sauerbrey equation will only hold when the deposited material is evenly distributed on, and rigidly attached to, the crystal surface. Furthermore, the adsorbed mass must be small (< 2 %) compared to the mass of the crystal.

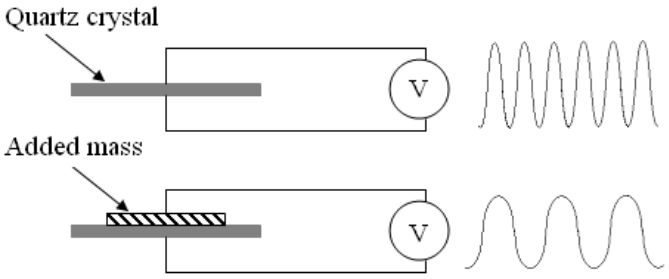

Fig. 19 Principle of the QCM sensing.
A voltage applied to the crystal makes it oscillate. An added mass on the crystal induces a decrease in the oscillation frequency.

As changes in frequency of a quartz crystal can be measured with high precision, this provides a very sensitive method (<1 ng/cm^2) to monitor thin film deposition in a liquid or gas medium, as well as to analyse the kinetics of adsorption/desorption of molecules at the interface between a solid and a solution.

V.6.2 The dissipation factor

Adding the dissipation factor (D factor) to the QCM technique enables extraction of physical properties (viscosity, density, shear modulus and thickness) of the material adsorbed to the crystal. The shear modulus is a quantity that measures stiffness of materials; it is defined as the ratio of shear stress to the displacement per unit of length. The D factor is the energy loss per oscillation as a fraction of the total energy stored in the system (multiplied two times by 2π). It is defined in equation Eq. 7.

Eq. 7

$$D = \frac{E_{lost}}{2\pi E_{stored}}$$

D = Dissipation factor
E_{lost} = Energy lost during one oscillation cycle
E_{stored} = Total energy stored in the oscillator

Dissipation occurs when the applied voltage on the electrodes of the crystal is shut off and the energy from the oscillating crystal dissipates from the system. It is quantified by measuring the time that the crystal needs to stop oscillating when the electrical excitation is stopped.

[65] Sauerbrey, G., *Verwendung von schwingquarzen zur wagung dunner schichten und zur mikrowagung*, Zeitschrift Fur Physik 1959) **155:** 206-222

If a thin and rigid film (such as a metal film) is attached to the crystal, a small fraction of energy is dissipated, resulting in a slow decay of the oscillation amplitude, and thus a low D factor (see Fig. 20.a). However, if a thick and viscous film (such as a polymer coupled with water) is attached to the crystal, a bigger fraction of energy is dissipated during each oscillation, resulting in a faster amplitude decay, and thus a higher D factor (see Fig. 20.b).

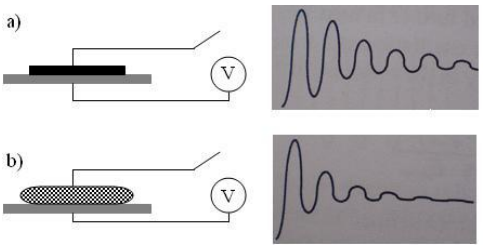

Fig. 20 Energy dissipation
A thin and rigid film (a) attached to a quartz crystal induces a small dissipation of energy A bigger fraction of energy is dissipated by a thicker and more viscous film (b) with a faster amplitude decay.

The D factor can be used to detect conformational changes adopted by macromolecules linked to the surface. For example, it has been reported that if elongated molecules adsorb flat on the surface, only low dissipation values will be observed. However, long molecules adopting a standing up position at the surface, will yield high dissipation values.[66]

Measuring the D factor simultaneously with the resonance frequency of the crystal allows accurate analysis of films that do not obey linear relation between change in frequency and change in mass. Knowing the magnitude of the dissipation factor adds an extra dimension to the classic QCM technique since it allows the determination of the viscoelastic properties of the adsorbed material, in addition to its mass.

In a QCM-D experiment, frequency and dissipation values at several overtones are collected. Data analysis is performed by studying changes in those values, and the difference of behaviour of these values between the different overtones. A frequency shift indicates a mass release or uptake, whereas a dissipation shift corresponds to change in the viscoelastic properties due to, for example, water uptake inducing a swelling phenomenon or water release inducing a collapse of the molecular structure.

It is important to emphasize that when a non rigid viscoelastic hydrogel is formed at the interphase, such as a hydrophilic polymer layer, the Sauerbrey equation does not hold. To calculate the four physical properties of such viscous adsorbed layers mentioned above (viscosity, density, shear modulus and thickness), a mathematical model, called Voigt viscoelastic model, is requested and needed to acquired frequency and dissipation data at least at two different overtones.

In a typical QCM-D experiment, frequency and dissipation shifts are monitored simultaneously in real-time while molecular layers are formed on a crystal surface. Fig. 21 shows a schematic drawing of what the QCM-D responses might look like during macromolecule adsorption and subsequent modification of the adsorbed macromolecules. Three main steps are imagined: first (1) the binding of small globular molecules induces a moderate frequency shift (mass uptake) and a low dissipation shift (rigid layer). Then (2) the binding of large elongated molecules induces the formation of a softer and

[66] Technology note; Q-sense, QS 407-01-2

thicker layer which can be seen by higher frequency and dissipation shifts. Finally (3) another step removes the elongated molecules, and frequency and dissipation shifts decrease and regain their initial values.

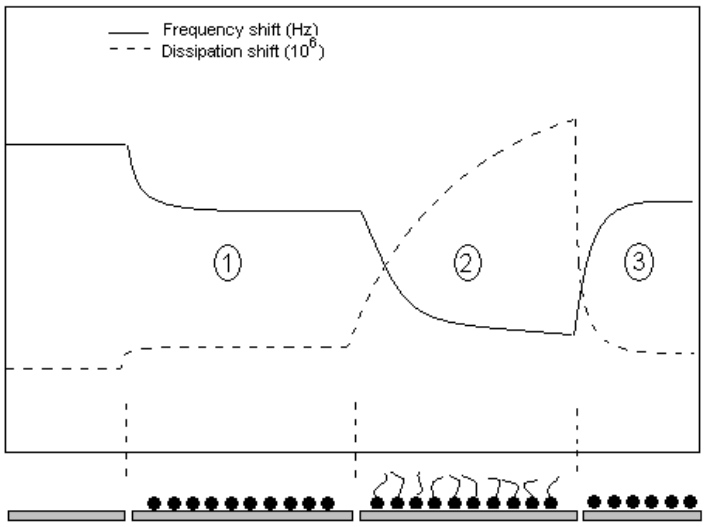

Fig. 21 Schematical representation of a QCM-D experiment

(1) Binding of a small globular molecule: Moderate frequency shift (mass uptake), and low dissipation shift (structural change)
(2) Binding of a large elongated molecule: Formation of a softer and thicker layer which can be seen by higher frequency and dissipation shifts.
(3) Rinsing with buffer: The elongated molecule is removed, frequency and dissipation decrease.

QCM-D is a powerful surface-based technique to study molecular adsorption and/or interaction processes on various surfaces (metals, polymers, functionalized and even nano-structured coatings). It is used to verify the specificity of interactions, to measure the thickness and hydration of deposited films, to characterize the affinity between a surface-bound receptor and a soluble ligand, to study the nature and the morphological state of the adsorbed species, etc. For example it is used to study conformational changes of polymers[67], to follow the cross-linking of polymeric film[68], to monitor protein adsorption kinetics[69-70] and cell adhesion and growth[71], to study binding kinetics of proteins to various surfaces[72], etc.

Given that the lower detection limit is around 1 Hz, which corresponds to a mass of 17.5 ng/cm², the sensitivity of the technique is around that value.

V.7 Reflectometry

In many situations, QCM-D data alone do not provide a complete description of the structure of the layer bound to the crystal surface. This is due to the fact that the mass measured by QCM-D also includes significant amounts of water molecules associated with the molecular layer (e.g., solution trapped inside

[67] Liu *et al.*, *Study of the Kinetics of the Pancake-to-Brush Transition of Poly(N-isopropylacrylamide) Chains*, Journal of Physical Chemistry B (2005) **47:** 22603–22607
[68] Hedin *et al.*, *Adsorption behavior and cross-linking of EHEC and HM-EHEC at hydrophilic and hydrophobic modified surfaces monitored by SPR and QCM-D*, Langmuir (2007) **23:** 6148-6155
[69] Hook, Rodahl et al., *Energy dissipation kinetics for protein and antibody-antigen adsorption under shear oscillation on a quartz crystal microbalance*, Langmuir (1998) **14:** 729-734
[70] Hook *et al.*, *Variations in coupled water, viscoelastic properties, and film thickness of a Mefp-1 protein film during adsorption and cross-linking: A quartz crystal microbalance with dissipation monitoring, ellipsometry, and surface plasmon resonance study*, Analytical Chemistry (2001) **73:** 5796-5804
[71] Modin C, S. A., Foss M, Duch M, Justesen J, Chevallier J, Andersen LK, Hemmersam AG, Pedersen FS, Besenbacher F, *QCM-D studies of attachment and differential spreading of pre-osteoblastic cells on Ta and Cr surfaces*, Biomaterials (2006) **8:** 1346-1354
[72] Kastl *et al.*, *Kinetics and thermodynamics of annexin A1 binding to solid-supported membranes: a QCM study.*, Biochemistry (2002) **31:** 10087-10094

and in between adsorbed molecules or lipid vesicles). Reflectometry is an optical technique used to study events at solid-liquid interfaces. Unlike QCM-D which measures the mass acoustically coupled to the sensor ($m_{acoustic}$, see paragraph VI.6), reflectometry measures changes in refractive index near the surface that result from the adsorption of compounds to the sensor (m_{optic}). m_{optic} is often assumed to be free from any interference of solvent, and it is sometimes referred to as dry mass.[73]

VI Materials and methods

Unless otherwise stated, all chemicals were obtained from commercial sources and were used without further purification. Water was filtered and deionised using a MilliQ purification unit (Millipore, France). Buffer 1 corresponds to PBS 10 mM phosphate, 137 mM NaCl, 2.7 mM KCl, pH 7.4 (tablets, Sigma Aldrich) whereas buffer 2 corresponds to a non isotonic buffer made of 2 mM phosphate, 10 mM NaCl, pH 7.4.

VI.1 Material preparation

VI.1.1 Vesicle preparation

POPC and/or POPC-POPS (3:1) (Avanti Polar Lipids Inc, USA) were first dissolved in chloroform at a concentration of 10 mg/ml. Stock solutions were stored under N_2 at -20°C. 6 mg of solubilised lipids were placed into a round-bottomed flask. Chloroform was evaporated under a low flow of nitrogen while the flask was rotated to obtain a thin lipid film on its walls. The flask was then connected to a vacuum pump (-95 kPa, at room temperature) for at least 1 hour to remove residual chloroform. The lipids were hydrated by addition of 1.2 ml of buffer 1 and mixed with a mini vortex shaker at 1600 rpm for approximately 1 min. Lipid suspensions in PBS were extruded with polycarbonate membranes (Whatman, USA) according to a two step procedure: a) 11 times through membranes with a porosity of 100 nm; 11 times through membranes having a porosity of 30 nm. An *Avanti* mini extruder® (Avanti Polar Lipids Inc, USA) was used for this purpose and the whole extrusion protocol was performed at room temperature. After extrusion, all vesicle solutions were stored at 4°C for maximum 1 month until use.

VI.1.2 Preparation of protein solutions

Chicken egg-white LYSO and OVA lyophilized proteins (Sigma Aldrich) were dissolved at room temperature during 2 hours in previously filtered (0.22 µm filters. Ref. Whatman, polyethersulfone membrane with polypropylene housing or Whatman, FP 30/0.2 CA-S) buffer 2 at a concentration of 1 mg/ml. The dissolution was performed adopting a rocking shaker (tilt angle ± 30°, frequency:

Fig. 22, Rocking shaker

[73] Edvardsson *et al.*, *QCM-D and Reflectometry Instrument: Applications to Supported Lipid Structures and Their Biomolecular Interactions*, Analytical Chemistry (2009) **81:** 349-361

1 move/sec, and a geometry of agitation as reproduced in Fig. 22). When possible, the protein solution was filtered. The solutions were aliquoted in sterile Eppendorf tubes and stored at -20°C. For some measurements (see result section), lyophilized OVA was dissolved either in milliQ water, in deionized water or in a Tris buffer (2 mM – pH 8.5) containing NaCl (10 mM). HI solution (2 mg/ml in buffer 2) was obtained from the ULg. Prior to use, all protein solutions were thawed and diluted to reach concentrations ranging from 15 µg/ml to 100 µg/ml. Delay between thawing and dilution was kept to approximately 10 min.

VI.1.3 Preparation of polycation solutions

10 mg of each polycation were dissolved for 2 hours at room temperature in buffer 2 at a concentration of 2 mg/ml, using a rocking shaker (the same way as for protein solutions, see previous paragraph) and a magnetic stirrer to prevent the polycation from sticking to the lid of the vial. pH was adjusted to 7.4 with HCl 0.1 M. The solutions were filtered through 0.22 µm filters (Whatman, polyethersulfone membrane with polypropylene housing, 25 mm diam; Batch X468), aliquoted in sterile Eppendorf tubes and stored at -20°C.

VI.1.4 Preparation of PEC solutions

PEC solutions were either prepared at Chalmers University of Technology at a concentration of 45 µg/ml or received from the ULg at a concentration of 450 µg/ml. The PEC suspensions were prepared according to a protocol optimized by the ULg.

VI.2 Solution characterization

VI.2.1 UV spectrophotometry

UV spectra of protein solutions (100 and 1000 µg/ml) were recorded with a UV/Vis/NIR spectrophotometer (Cary 5000, Varian). The scan speed was 600 nm/min, and the scan resolution was < 0.05 nm. Absorbance was measured for wavelengths ranging from 200 to 300 nm with a 1 cm light path. Between measurements, the quartz cuvette was rinsed with acetone and milliQ water and dried under a flow of nitrogen.

VI.2.2 Dynamic Light Scattering

Particle sizes were determined by DLS with a Zetasizer Nano ZS (Malvern Instruments Ltd). The measurements were performed at 22°C on protein, polycation and PEC solutions at concentrations ranging from 15 µg/ml to 1 mg/ml.

VI.2.3 Zeta Potential

ZP measurements were performed with a Zetasizer Nano ZS (Malvern Instruments Ltd). The measurements were performed at 22°C on polycation and PEC solutions at concentrations ranging from 30 to 90 µg/ml. ZP measuring cell was rinsed with 2 ml of ethanol, 5 ml of milliQ water and 1 ml of

buffer between measurements.

VI.2.4 Nanoparticle Tracking Analysis

NTA measurements were performed with a Nanosight instrument (model LM10, NanoSight Ltd, London) at room temperature on vesicle, protein, polycation and PEC solutions (see descriptions above), at concentration ranging from 15 µg/ml to 1 mg/ml.

VI.3 Interaction analysis with Quartz Crystal Microbalance with Dissipation monitoring

QCM-D measurements were performed at several harmonics (n = 3, 5, 7, 9, 11 and 13) at 22°C using a Q-Sense instrument and 5 MHz SiO_2 coated quartz crystals (Q-Sense AB, Sweden). Prior to use, the crystals were cleaned in 10 mM SDS, rinsed with water, dried under a flow of nitrogen and exposed to UV for 30 min. Measurements were performed using a flow rate of either 100 µl/min or 75 µl/min and a temperature of 22°C. The lipid concentrations used were: POPC 0.1 mg/ml (in buffer 1); POPC:POPS (3:1) 0.1 mg/ml (5 mM $MgCl_2$ was added to buffer 1 to enhance the kinetic of the bilayer formation process); PECs 45 µg/ml; polycations 30 µg/ml; ternary compound 30 µg/ml. The delay between bilayer formation and injection of samples was approximately 10 min. All QCM-D data are presented for the 9^{th} overtone. Frequency shifts were normalized to the fundamental frequency of the crystal by division of the frequency shift by the overtone number of the resonant frequency. Data analysis, plotting and modeling were realized using Q-Tool software (Q-Sense AB, Göteborg, Sweden).

VII Results

This section will first describe results from characterization of protein (LYSO, OVA, HI), polycation, PEC and lipid vesicle solutions. Next it will present the data collected from the QCM-D measurements.

VII.1 Protein characterization

VII.1.1 Lysozyme

LYSO solutions were characterized by DLS, NTA and UV spectroscopy. The DLS measurement was performed on a 1 mg/ml LYSO solution in buffer 1. Fig. 23 shows that adopting the Cumulant method [74] this deconvolution method fits well to DLS raw data. From the monoexponential decay of this curve, it allows to derive the existence of one single peak with a mean hydrodynamic diameter of the protein of 5.7 nm. This value is in agreement with previous data.[75]

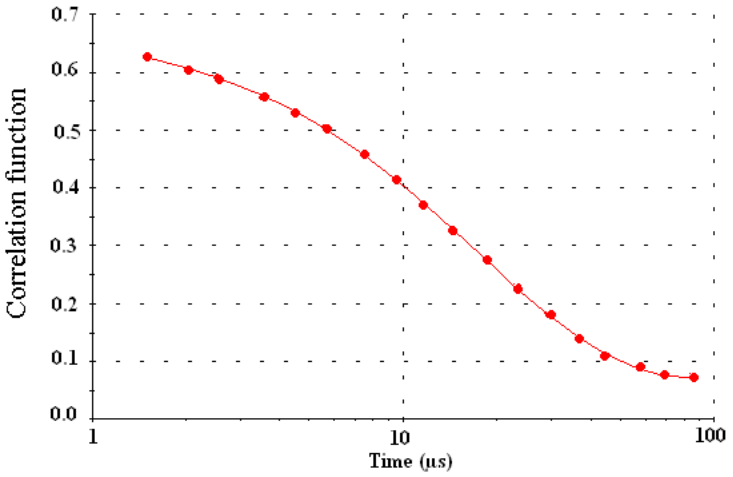

Fig. 23
Cumulant fit for a 1 mg/ml LYSO solution measured by DLS in buffer 1.

In spite of a low detection limit of about 35 nm, NTA was also adopted to verify the possible existence of aggregates in the LYSO solutions. These measurements (see Fig. 24) highlighted the presence of a small degree of aggregation in three LYSO solutions at three different concentrations: 30, 100 and 1000

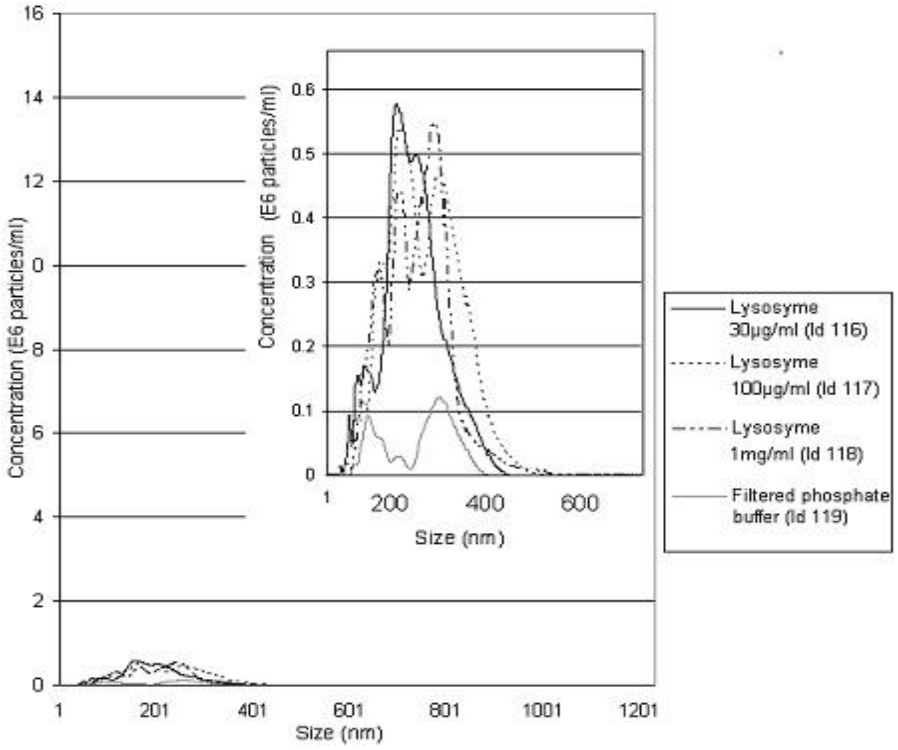

Fig. 24
Size distribution of LYSO solutions measured by NTA at different concentration, based on two measurements

[74] Koppel and Dennis, *Analysis of Macromolecular Polydispersity in Intensity Correlation Spectroscopy: The Method of Cumulants*, The Journal of Chemical Physics (1972) **57:** 4814
[75] Application note from Malvern Instrument http://www.malvern.com/common/downloads/campaign/MRK414-01.pdf Accessed the 28th of June, 2010.

µg/ml. The size of the aggregates ranged from 100 nm to 250 nm, independently of the LYSO concentration. In brief, a very good agreement was found between the DLS and the NTA results. Note that NTA seems more sensitive to detect small aggregates/contaminant particles.

VII.1.2 Ovalbumin

At the very beginning of the project, we had to face a surprising variability in dissolution state of OVA. Either we obtained true solutions in which any aggregates (>~50 nm) could be detected by NTA, or 0.22 µm filters were blocked after injection of a few ml of the protein solution. In the latter case, the retentate was analysed with NTA. Fig. 25 shows typical pictures of OVA aggregates detected with NTA. The NTA results, summarized in Fig. 26 and in Table 1, unexpectedly showed that the filtered OVA solutions contained much more aggregates than the non filtered solutions.

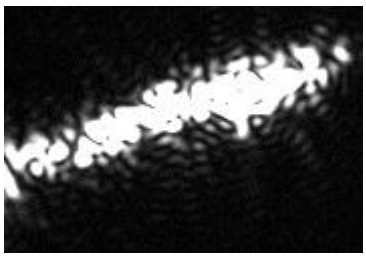

Fig. 25
OVA aggregate detected by NTA

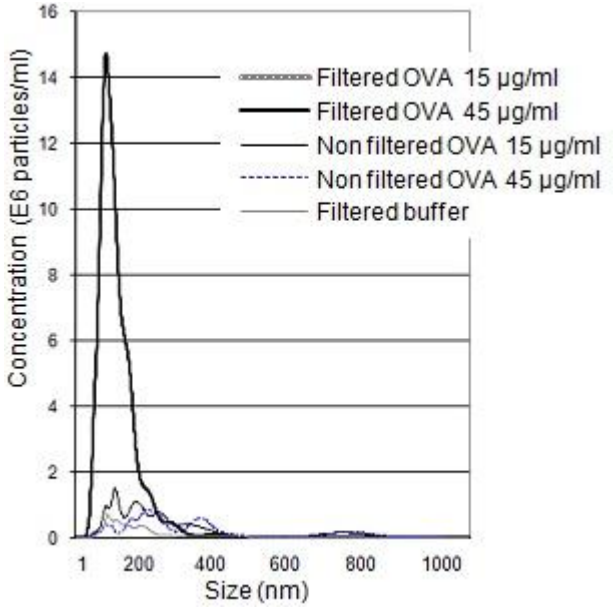

Fig. 26
Size distribution of OVA solutions measured by NTA

Table 1
Volume (%) and number of OVA aggregates in 1 ml of solution

	Volume (% in 1 ml)	**Number of aggregates /ml**
Filtered OVA 15 µg/ml	9.8×10^{-15}	9.4×10^{8}
Filtered OVA 45 µg/ml	7.0×10^{-14}	1.1×10^{9}
Non filtered OVA 15 µg/ml	1.7×10^{-14}	2.3×10^{8}
Non filtered OVA 45 µg/ml	1.5×10^{-14}	1.7×10^{8}
Filtered buffer	6.1×10^{-13}	6.1×10^{7}

With a view to highlight the origin of these protein aggregates, we have assessed the following parameters in order to improve the dissolution state of the protein; (i) protein batch, (ii) pH of the dissolution medium, (iii) mixing mode, (iv) protein concentration, (v) time.

To modify the ionisation status of the protein, we have compared the dissolution states of OVA in buffer 2 (pH 7.4) and in a Tris buffered at pH 8.5 (10 mM NaCl). NTA size distribution reported on Fig.

27 A and Fig. 27 B indicated that, at both pH, the bigger the concentration, the bigger the total amount of aggregates. If the adoption of a more alkaline buffer prevents partially the protein aggregation (comparison between Fig. 27 A and B), the presence of such a high content of protein aggregates does not fit with a true solution as we have observed for LYSO Fig. 24).

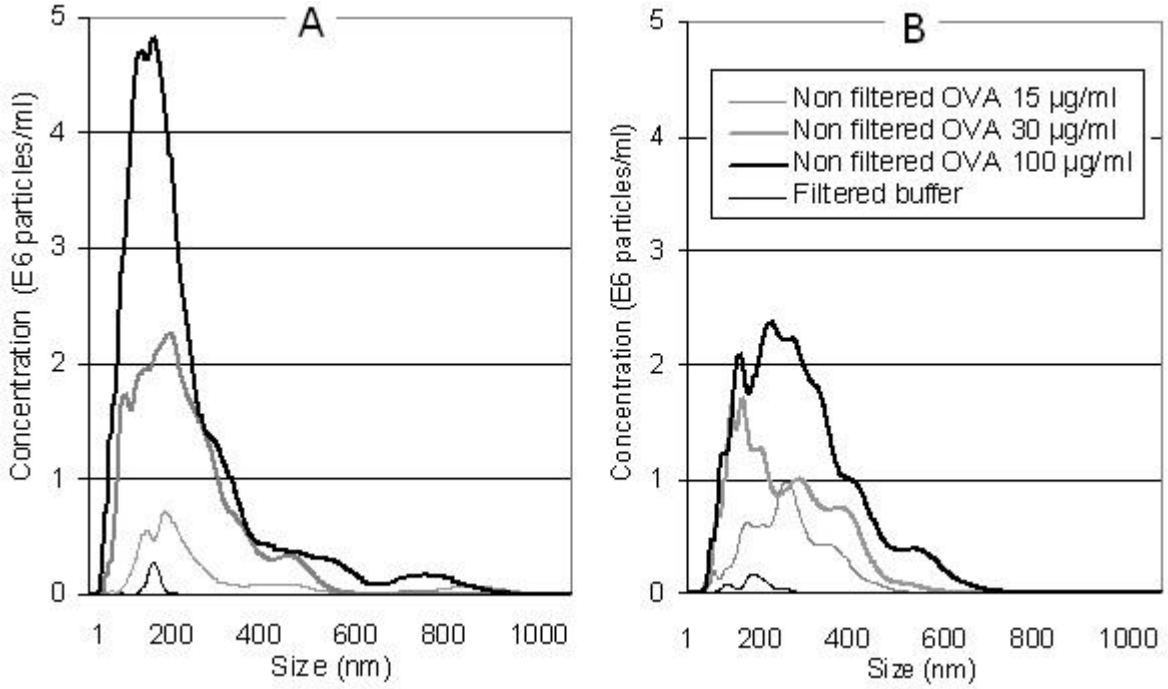

Fig. 27
NTA size distribution of OVA solutions either in phosphate buffer pH 7.4 (A) or Tris pH 8.5 (B).

Next, the role of the mixing was investigated. The following 4 different dissolution conditions at two concentrations (15 and 30 µg/ml) were compared:

1) Dissolution (2 hours) with mixing on a rocking shaker followed by filtration (see Fig. 22, p 26)
2) Dissolution (2 hours) without mixing on a rocking shaker followed by filtration
3) Dissolution (2 hours) with mixing on a rocking shaker
4) Dissolution (2 hours) without mixing on a rocking shaker

The overall conclusion from this study was that we were unable to find favourable conditions to avoid OVA aggregation. Unexpectedly sometimes the filtered solutions contained more aggregates than the non filtered ones. Mixing during the sample preparation did not reproducibly improve the state of dissolution of the protein.

Additionally, the aggregation process was further studied as a function of time. Already directly after gentle mixing of the solution, to prevent OVA to stick to the vial wall, the solution looked clear to the naked eye, as well as after a 15 minutes' mixing on a rocking shaker (see Fig. 29a); after 30 minutes' mixing the presence of OVA aggregates in the solution was easily visible to the naked eye (see Fig. 29b). As an additional characterization analysis, UV measurements were also performed to detect aggregation. With this technique, a possible presence of aggregated proteins results in a signal decrease. The results of

these measurements are plotted in Fig. 28.

This aggregation process was also followed by NTA, but these two granulometric techniques were found to be inadequate to analyse precisely so big aggregates. Fig. 30 shows the cumulant fit plot for a DLS measurement on an OVA solution (15 µg/ml). Given the bad quality of the fitting, several other ones were tested. However, they all contained a major part where no equation was good enough to make the measured data fit to the model calculation.

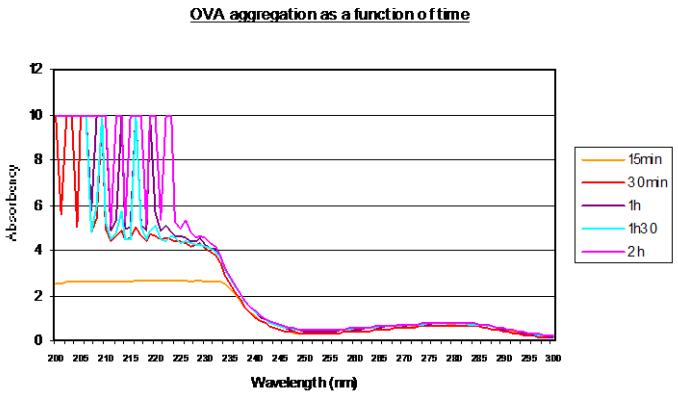

Fig. 28
UV measurements of an OVA solution at different time during the dissulution process. The profile of the curve at 15 min is different of all the other ones. There is no aggregation detected at that time.

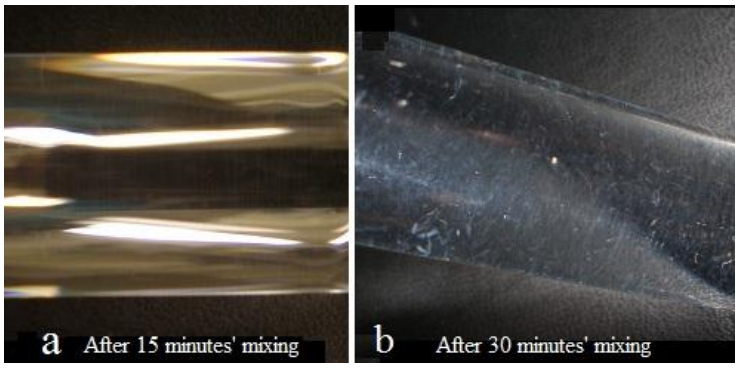

Fig. 29
OVA aggregates appear after 30 minutes' mixing

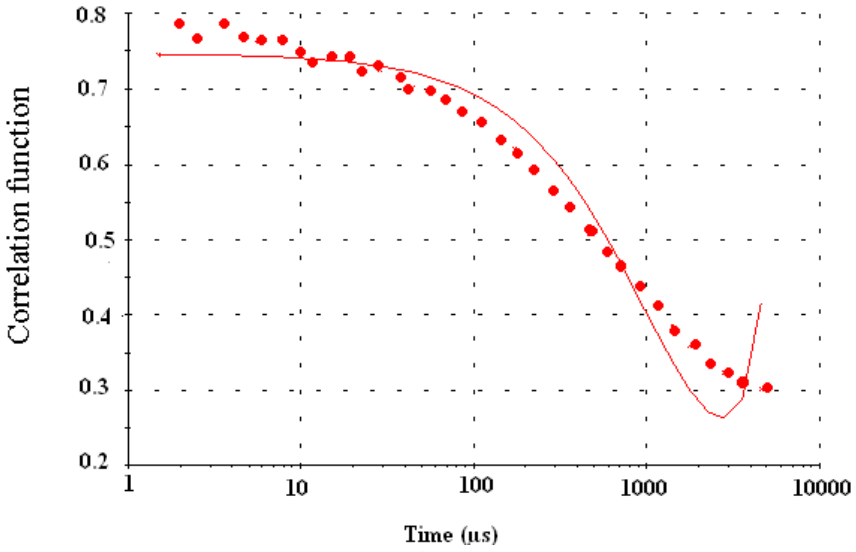

Fig. 30
Cumulant fit of DLS data acquired on a 100 µg/ml OVA solution dissolved in filtered buffer 1.

Parallel experiments were realized at ULg and confirmed the influence of the mixing factor on the OVA aggregation phenomenon.[76]

VII.1.3 Human insulin

The analysis of the DLS data, acquired with a 1 mg/ml HI solution in buffer 1, provides a mean protein diameter of 17.3 nm, with, however, an unsatisfactory fitting of the autocorrelation curve by the Cumulant method. Although measurements were repeated using different settings (scanning time, fitting algorithm, number of measurements), data deconvolution could not be improved. NTA analysis showed that HI solution was free of aggregates. Thus, for HI, the protein size distributions by both techniques were similar to those obtained with LYSO (see Fig. 23), as opposed to what is obtained with OVA solutions. Since no large aggregates were present, the poor quality of the DLS data might be due to the presence of dimers or trimers of the protein in the solution.

VIII Polycation characterization

In order to make PECs by electrostatically assembling polycations and proteins, we used 4 polycations of different Mn (see section IV.6 Polycations, p. 13). They were dissolved in buffer 1. To characterize them, NTA, DLS and ZP measurements were performed. No aggregates were detected by NTA and DLS for the four polycation solutions (data not shown). ZP data, collected in Table 2, show that the 4 polycations were weakly positively charged (between 0.8 and 4.7 mV).

IX Selection of good quality material for PEC preparation

At the outset of the project, the ambition was to prepare PECs containing OVA for interaction analysis with lipid membranes. Starting from an aggregated OVA solution prepared according a protocol given by ULg (see Material and methods, paragraph VI.1.2), we tried to prepare such PECs. However, given the difficulties met with OVA dissolution, DLS and NTA measurements did not yield encouraging data. The comparison of the NTA size distribution of PECs either loaded with OVA or HI (Fig. 31 A and Fig. 31 B respectively) allows to conclude that the total amount of PECs formed after a duration of about 1 hour was significantly larger with HI than in the presence of OVA. Therefore, we decided to continue working with PECs loaded with HI.

[76] Influence of agitation mode on OVA dissolution state, 2010, University of Liège

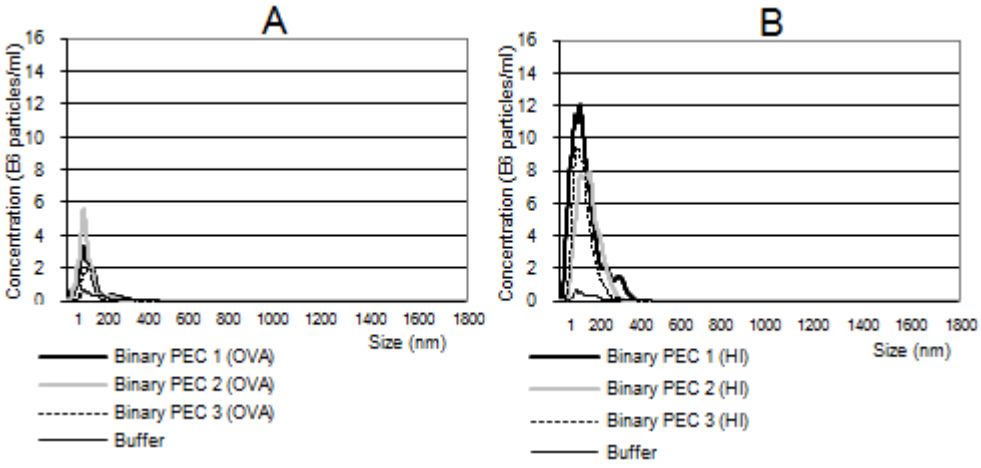

Fig. 31
NTA size distribution of binary PEC 1, 2 and 3 suspensions, either with OVA (A) or with HI (B)

To focus our attention on the main aim of our work, i.e. interaction of PECs with lipid monolayers, the ULg provided us directly with the nanomaterials according to the following list:

- 4 types of PEC prepared by assembling the same 4 polycations as the ones cited above with HI. These NPs were also denoted PEC 1, 2, 3 and 4.
- 2 types of PEC containing a ternary compound: ternary PEC 1 and 2. The presence of that compound is supposed to prolong the stability of the preparation.
- 3 control solutions: ctrl ternary PEC 1 and 2 without HI, and the ternary compound alone.

X PEC Characterization

X.1 Zeta potential measurements

Table 2 shows that both binary and ternary PECs were clearly positively charged (around 20-25 mV), whereas the ternary compound alone displayed a negative electrokinetics potential (at -43.2 mV).

Table 2

ZP values of polycations and PECs in buffer 1, of POPC vesicles in buffer 2, and of POPC-POPS (3:1) vesicles in buffer 2 containing $MgCl_2$ 5 mM

	ZP (mV)
Poycations	
Polycation 1	+1.6
Polycation 2	+0.8
Polycation 3	+4.7
Polycation 4	+3.9
PECs	
Binary PEC 1	+26.3
Binary PEC 2	+25.3
Binary PEC 3	+25.4
Binary PEC 4	+21.2
Ternary PEC 1	+25.1
Ternary PEC 2	+21.8
Controls	
Ctrl ternary PEC 1 without HI	+7.9
Ctrl ternary PEC 2 without HI	+9.0
Ternary compound	-43.2
Lipid vesicles	
POPC vesicles	+0.7
POPC-POPS (3:1) vesicles	-21.4

X.2 Size measurements

Size measurements of polycations and PECs were achieved with both DLS and NTA within 1 week after sample reception. DLS data plotted in Fig. 32 show that binary PECs 1, 2 and 3 had all a mean diameter close to 200 nm, whilst the size of ternary PECs was higher. Ternary PEC 1 is about 350 nm in diameter whereas ternary PEC 2 measures about 650 nm in diameter. NTA data plotted in Fig. 33 show that binary PEC solutions 1, 2 and 3 present well defined size distributions having a mean diameter, for binary PECs 1 and 2, of about 200 nm, and for binary PECs 3, of about 170 nm. Both DLS and NTA show binary PECs 4 as being very polydisperse. DLS does not yield a reliable result for those binary PECs, while no binary PECs are detected by NTA. Table 3 summarizes both types of data. As no significant amount of aggregates was detected in polycation solutions, the polycations were all characterized as well solubilized. Given the low polydispersity index values and mean sizes of around 200 nm, we considered the binary PECs as being well stabilized, with the exception of binary PEC 4 that formed bigger and fewer aggregates than expected. The ternary PECs were not characterized as being as well stabilized as the ones without the ternary compound, given that their size distribution was much larger than the size distribution of the PECs without the ternary compound. Nevertheless, they had a good enough quality to be used in interaction studies with SLBs.

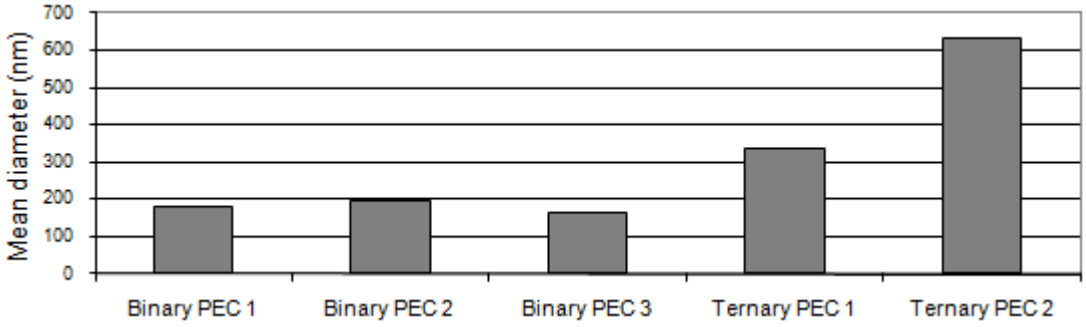

Fig. 32

Mean diameter of binary and ternary PECs measured by DLS.

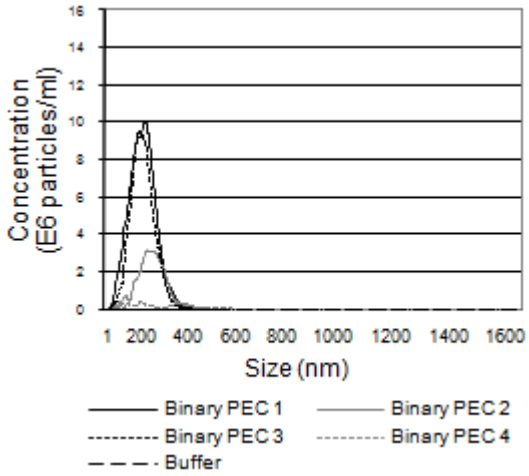

Fig. 33

NTA size distribution of the 4 types of binary PEC.

Table 3

Collected DLS and NTA mean diameter data for polycations, binary and ternary PECs, control samples and lipid vesicles. n.s. = sample not suitable for DLS measurement

	Mean diameter (DLS)	**Polydispersity index (DLS)**	**Mean diameter (NTA)**
Polycations			
Polycation 1 (Mn=90000)	n.s.	n.s.	No aggregates >~50nm detected
Polycation 2 (Mn=40000)	n.s.	n.s.	No aggregates >~50nm detected
Polycation 3 (Mn=20000)	n.s.	n.s.	No aggregates >~50nm detected
Polycation 4 (Mn=10000)	n.s.	n.s.	a few aggregates >~50nm detected, but negligible
PECs			
Binary PEC 1	178 nm	0.126	196 nm
Binary PEC 2	194 nm	0.128	206 nm
Binary PEC 3	166 nm	0.118	168 nm
Binary PEC 4	Not reliable	1	aggregates ranging from 50 to 460 nm
Ternary PEC 1	339 nm	0.179	aggregates ranging from 50 to 500 nm
Ternary PEC 2	633 nm	0.623	aggregates ranging from 50 to 500 nm
Controls			
Ctrl ternary PEC 1 without HI	n.s.	n.s.	nothing >~50nm detected
Ctrl ternary PEC 2 without HI	n.s.	n.s.	almost nothing >~50nm detected
Ternary compound	Not measured	Not measured	aggregates ranging from 50 to 300nm
Lipid vesicles			
POPC vesicles	109 nm	0.078	Not measured
POPC-POPS (3:1) vesicles	98 nm	0.066	Not measured

XI Lipid vesicle characterization

The ZPs of the different vesicles, extruded as described in paragraph V.1, are listed in Table 2 p. 35. While the ZP varied with the nature of the lipid used, the mean size of both types of vesicles was about the same (103.5 ± 5.5 nm), with a PdI (Polydispersity Index) close to 0. POPC vesicles were close to neutral, having a ZP close to 0 mV. The ZP of negatively charged vesicles containing 25% POPS (POPC-POPS 3:1) was -21.4 mV. These results are in accordance with previous data. [77-78]

XII Bilayer formation

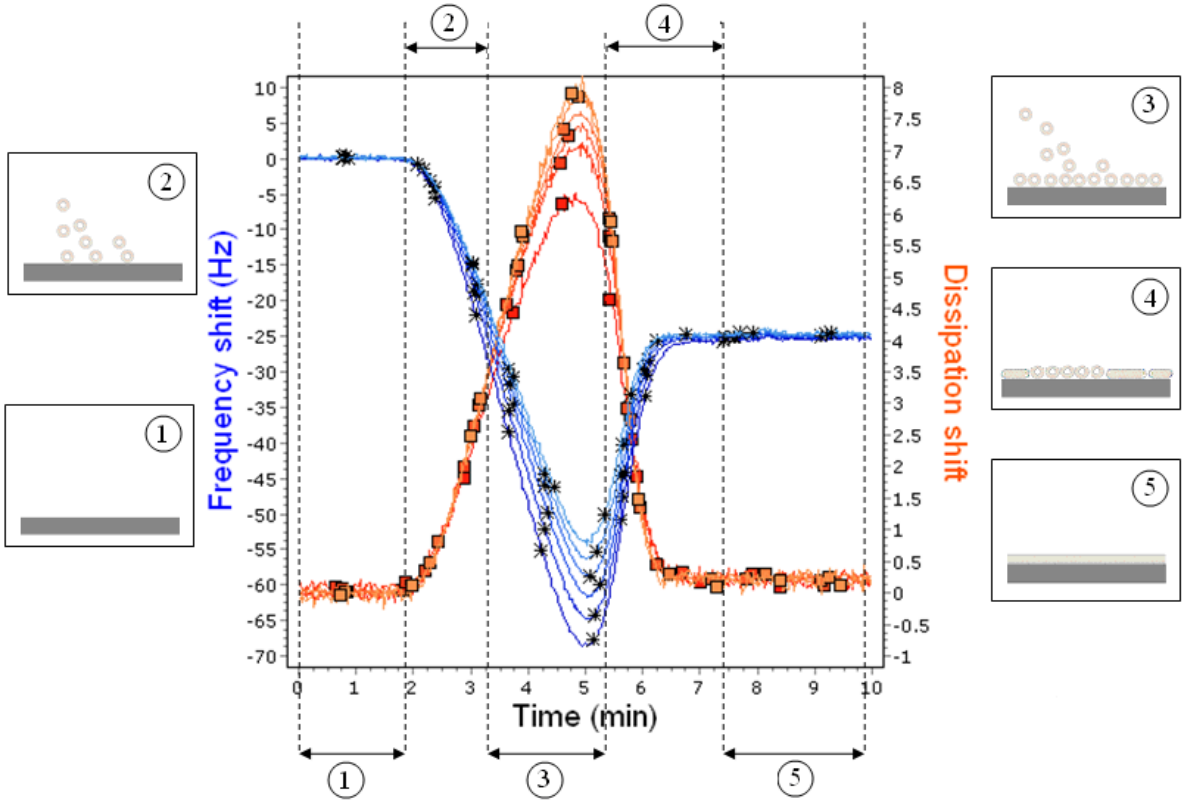

Fig. 34
Typical time curves of frequency shift and dissipation shift for a SLB formation measurement with the QCM-D technique.

The Fig. 34 is a typical QCM-D plot showing the formation of a SLB. Both frequency and dissipation shifts are plotted for all overtones registered.

(1) At the beginning, when there are no vesicles in contact with the quartz crystal, both frequency and dissipation shifts have a null value.

(2) When lipid vesicles are added onto the crystal, they start to adsorb onto it. There is decrease in frequency indicating a mass uptake (see QCM-D theory), and an increase in dissipation indicating the

[77] Kunze *et al.*, *Lipid Transfer between Charged Supported Lipid Bilayers and Oppositely Charged Vesicles*, Langmuir (2009) **25:** 5146-5158
[78] Frost R., G. C., Cerba B, Kasemo B, Svedhem S, *Structural rearrangements of polymeric insulin-loaded nanoparticles interacting with surface-supported model lipid membranes*, Colloids and Surfaces B-Biointerfaces (submitted) (2010)

formation of a viscoelastic structure onto the crystal.

(3) More lipids are adsorbed, making the frequency decrease and the dissipation increase, until they reach a critic surface coverage.

(4) At that critical step, vesicles start to rupture and to form some patches, releasing all molecules of water that were trapped inside the vesicles. This process makes the frequency increase indicating a mass loss due to all molecules of water that are released; and it makes the dissipation decrease indicating a decrease in the viscoelastic character of the adsorbed layer.

(5) At last, membrane patches merge together and form a bilayer. The frequency and dissipation shift obtained in this specific experiment were respectively of about 60 Hz and $7x10^6$. This is typically what is reported in the literature.[78]

XIII Quartz Crystal Microbalance with Dissipation monitoring data

SLBs of different compositions and charges were prepared as described in previous studies.[78]

XIII.1 Interaction between polycations and SLBs

On the negatively charged SLB (POPC-POPS 3:1), all 4 polycations showed the same adsorption profile. Fig. 35 shows QCM-D data in the form of frequency and dissipation shifts for all overtones upon injection of polycation 1 (Mn: 20000 Da), which is taken as an example. The frequency shift is about 20 Hz and is directly proportional to the mass adsorbed to the SLB through the Sauerbrey equation (Eq. 6 p. 23). The dissipation shift is close to 0, this value is related to the viscoelastic properties of the adsorbed layer (see experimental techniques). The dissipation shift is very low, indicating the formation of a rigid film. The adsorption of polycation to the SLB is irreversible, as observed from the stable frequency and dissipation shifts upon rinsing (see Table 4).

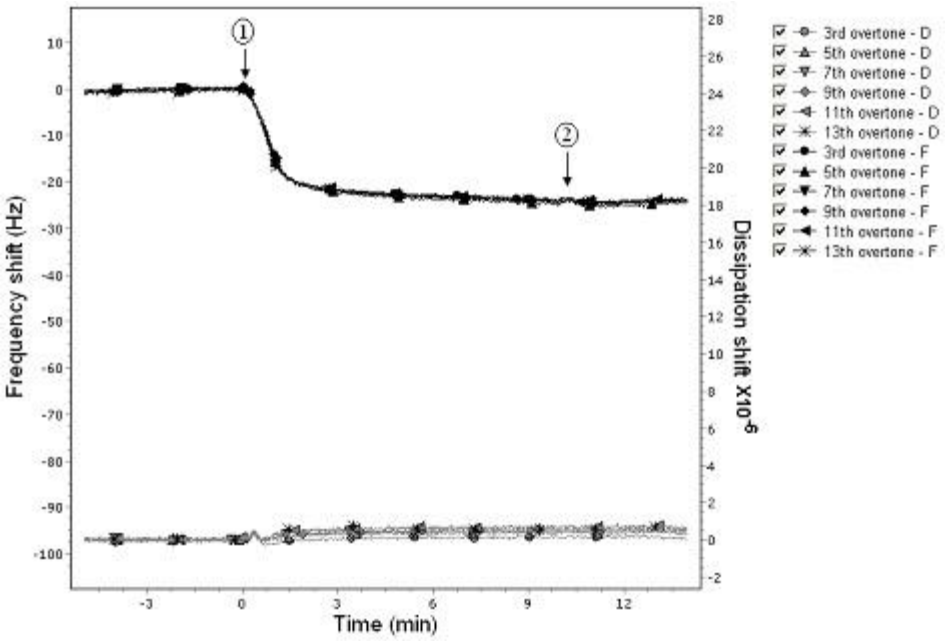

Fig. 35
QCM-D measurement showing the change in frequency and dissipation shifts upon adsorption of polycation 1 on a negatively charged bilayer made of POPC-POPS (3:1). Arrows indicate (1) polymer adsorption and (2) rinsing with buffer.

Table 4

Frequency and dissipation shifts for the 9th overtone upon rinsing after polycation adsorption on both neutral and negatively charged SLBs

	POPC-POPS (3:1)		POPC	
	Frequency shift	**Dissipation shift**	**Frequency shift**	**Dissipation shift**
Polycation 1	0±0	0.2±0.2	-1±2	0.2±0.4
Polycation 2	0±0	0±0	-0.5±1.2	0.4±0.3
Polycation 3	0±0	0±0	-0.2±0.3	0±0
Polycation 4	0±0	0±0	0±0	0±0

When adsorbed to the neutral SLB, polycations behaved differently. Fig. 36 shows that on the neutral SLB (POPC), all four polycations have much higher frequency and dissipation shifts than on the negatively charged SLB, although they had different adsorption profiles. As opposed to the negatively charged SLB on which polycations adsorbed completely irreversibly, polycations adsorbed to the neutral SLB with a low degree of reversibility (see Table 4).

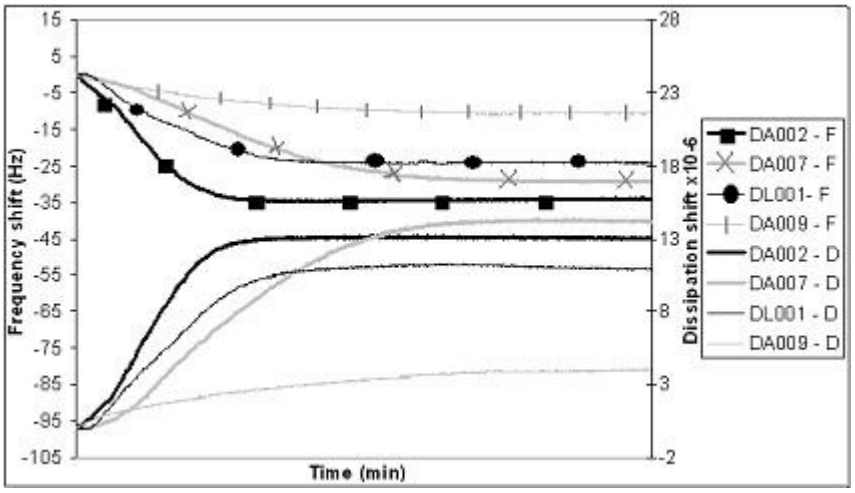

Fig. 36

QCM-D measurement showing the change in frequency and dissipation shifts upon adsorption of the polycations 1, 2, 3 and 4 on a neutral bilayer made of POPC

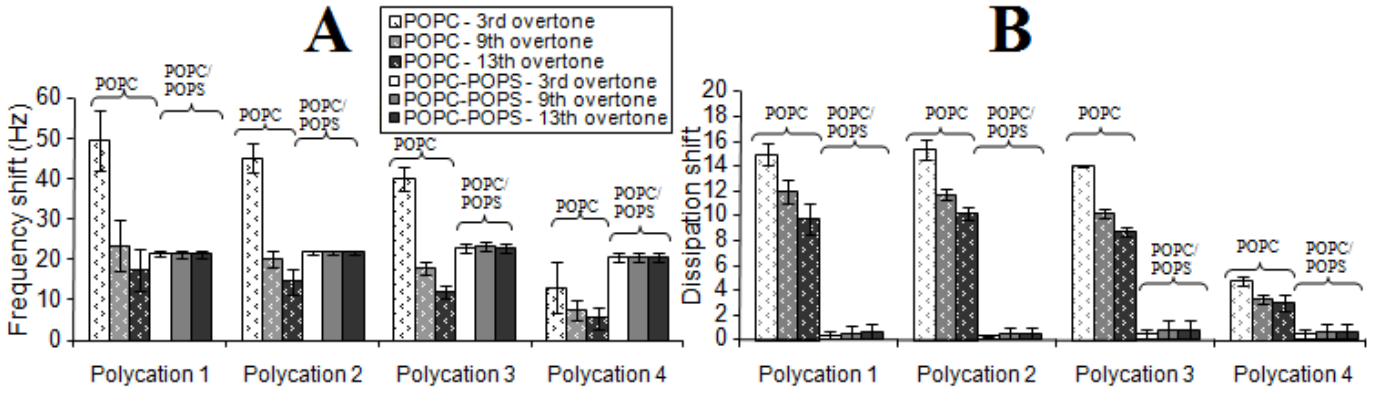

Fig. 37

Collected average frequency (A) and dissipation (B) shift values and standard deviations of 4 polycations at equilibrium, based on 2 to 4 measurements on two types of SLB

All polycation adsorption data are summarized in Fig. 37 A and Fig. 37 B to allow a comparison between results obtained at different overtones. Both graphs show that the adsorption of the four polycations on a negatively charged SLB yielded no spreading between the frequency and dissipation shifts obtained at different overtones. Using that SLB, the frequency and dissipation shifts were about 20 Hz and close to 0, respectively. On the contrary, those two graphs show that, when adsorbed to the neutral SLB, all polycations yielded significant spreading between measurements at different overtones and much higher dissipation shifts, indicating the formation of viscoelastic layers.

Furthermore, frequency and dissipation shifts upon rinsing are summarized in Table 4 for the layers of

the four polycations adsorbed on both neutral (POPC) and negatively charged (POPC-POPS 3:1) SLBs. Each value is equal or close to 0, meaning that the rinsing step did not induce any removal of, or any structural changes in the adsorbed polymeric material.

XIII.1.1 Calculation of the mass of the adsorbed polycation layers

In QCM-D, rigid films are characterized by low dissipation shifts. For such systems, the mass of the adsorbed layer is proportional to the frequency shift and can be calculated with the Sauerbrey equation. Given that the dissipation shifts were not low enough for polycation layers formed on neutral SLB, Voigt model has been adopted (using the Q-Tool software) instead of the Sauerbrey equation. The density of both the adsorbed layer and the buffer was assumed to be 1060 kg/m³, and the viscosity of the buffer was assumed to be 0.001 kg/m.s. In general quite good fittings were obtained (chi²<3.2) except for polycation 3 (chi² = 5.2). Masses of all adsorbed polycation layers are summarized in Fig. 38. They are all measured at equilibrium. It shows that, in general, the mass of all polycation layers adsorbed on the negatively charged SLB was about 400 ng/cm², except for polycation 3 layers. It also shows that on the neutral SLB, polycation 1 and 2 layers had a mass of about 700 to 800 ng/cm² whereas polycation 4 layer had a mass of about 400 ng/cm². Calculations did not yield a reliable mass value for polycation 3 layers.

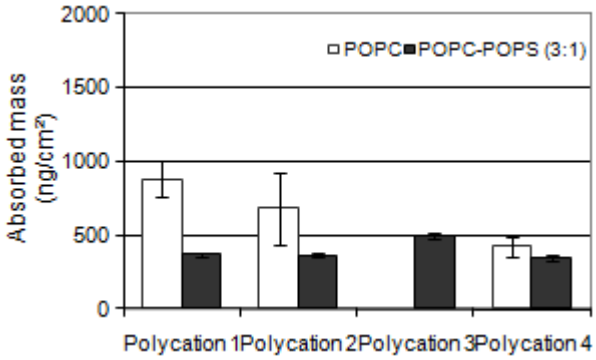

Fig. 38
Mass of the adsorbed polymer layers calculated using either Sauerbrey equation for the layers adsorbed on POPC-POPS SLB, either Voigt-based model for layers adsorbed on POPC.

XIII.2 Interaction between binary PECs and SLBs

Data for the adsorption of binary PEC 1 on both types of SLB were similar to previous data reported elsewhere.[78]

Exception made of PEC 4, all binary PECs yielded similar adsorption profiles on the negatively charged SLB. A trend was observed with respect to Mn. The higher the Mn of polycation used for PEC preparation, the higher the dissipation shift. Note that the frequency and dissipation shift values yielded by binary PEC 4 are similar to the value yielded by the polycations alone.

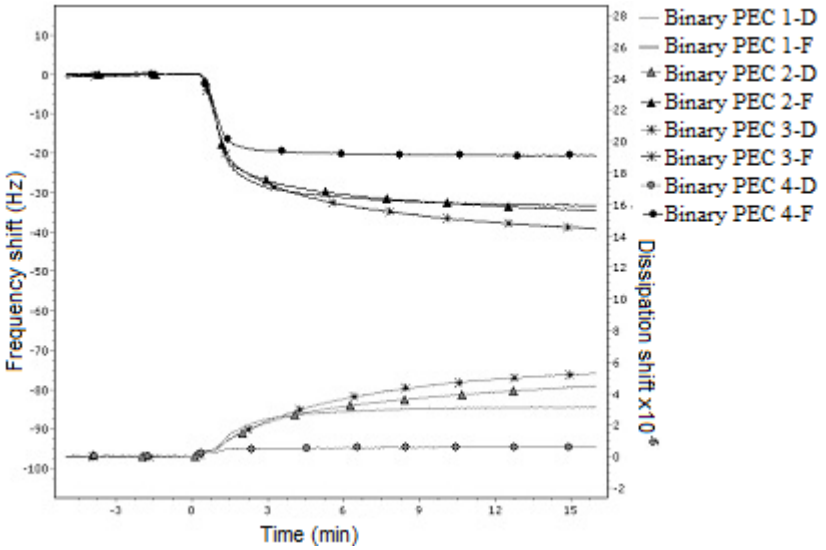

Fig. 39
Frequency and dissipation shifts (for the 9th overtone) during adsorption of binary PEC 1, 2, 3 and 4 on a negatively charged SLB made of POPC-POPS (3:1).

On the neutral membrane, only the binary PECs 1 were investigated. Fig. 40 shows that these PECs produced high frequency and dissipation shifts. This interaction profile is in accordance with data previously reported.[78]

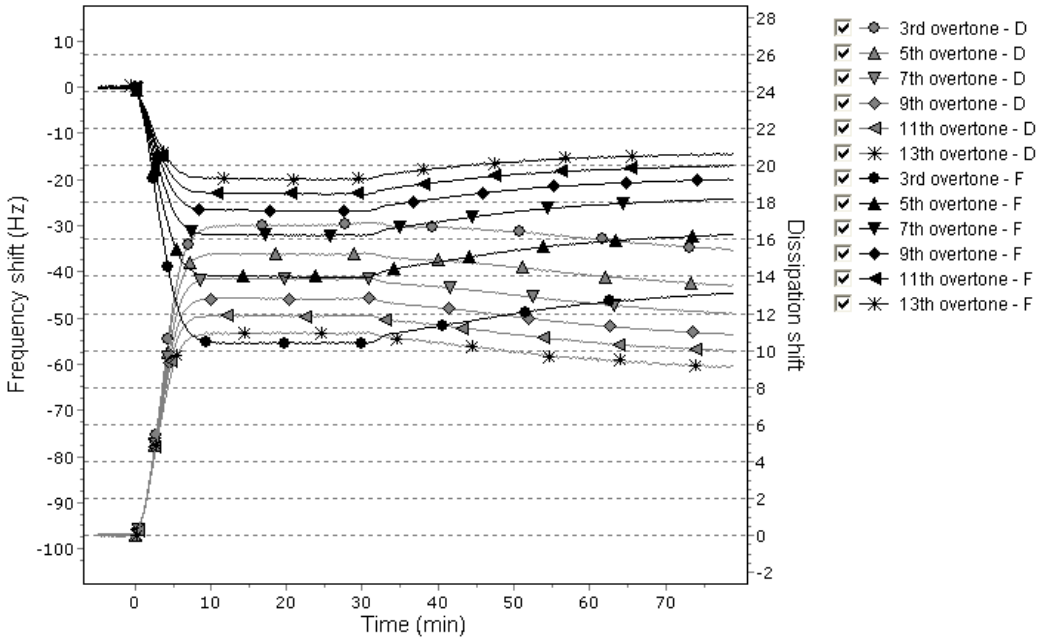

Fig. 40
Frequency and dissipation shifts for all overtones during adsorption of binary PEC 1 on a neutral SLB made of POPC

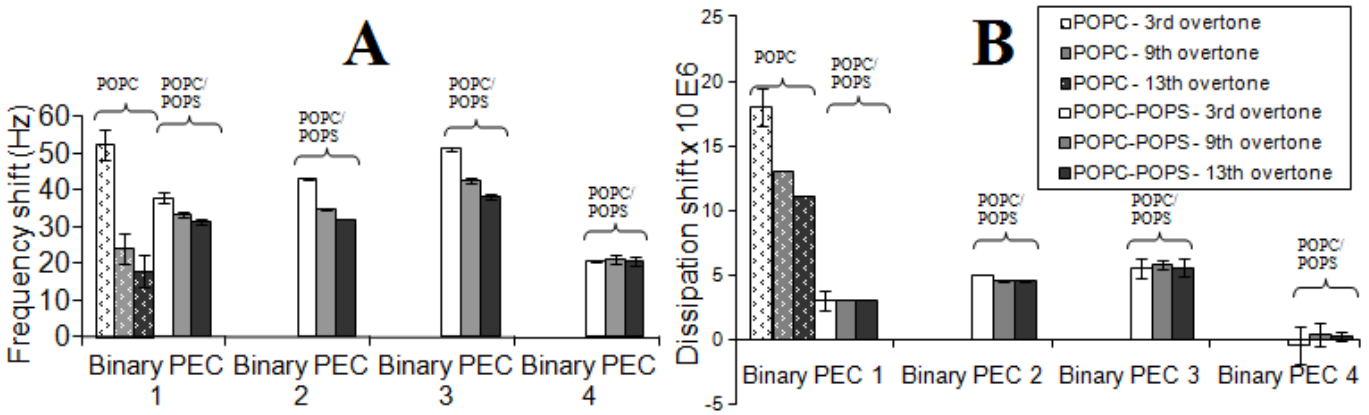

Fig. 41

Frequency (A) and dissipation (B) shifts for the 3rd, 9th and 13th overtones for binary PEC 1, 2, 3 and 4, based on 2 to 4 measurements.

Fig. 41 shows frequency and dissipation shift values at different overtones for the four types of binary PEC adsorbed on the negatively charged SLB, and for one type of binary PEC adsorbed on the neutral SLB. On the neutral SLB, measurements of binary PEC 1 at different overtones spread for both frequency and dissipation shifts. On the negatively charged SLB, measurements of all binary PECs but number 4 yielded a spreading between the different overtones only for the frequency shift curves. Note that binary PEC 4 showed the same frequency and dissipation profiles as the polycation alone.

Table 5

QCM-D shifts for the 9th overtone upon rinsing after binary PEC adsorption on both neutral and negatively charged SLBs

	POPC		**POPC-POPS (3:1)**	
	Frequency shift	**Dissipation shift**	**Frequency shift**	**Dissipation shift**
Binary PEC 1	7.3±0.4	-2±0	8±2.1	-2.4±0.5
Binary PEC 2	Not measured	Not measured	10.5±0	-3.8±0.4
Binary PEC 3	Not measured	Not measured	16.8±0.4	-5.5±0.4
Binary PEC 4	Not measured	Not measured	-1.5±0	0±0

Frequency and dissipation shift values between equilibrium and rinsing step are summarized in Table 5 for the four PECs adsorbed on both types of SLB. The adsorption of binary PEC 1 on both SLBs is predominantly irreversible, which is in accordance with previous data.[78] So it was for binary PEC 2. These two types of PEC formed a relatively stable layer on the SLBs. However, binary PEC 3 showed higher frequency and dissipation shifts upon rinsing on a negatively charged SLB, indicating a loss of mass due to a half reversible adsorption. Binary PEC 4 formed a stable layer on the negatively charged SLB, indicating that its adsorption was irreversible.

XIII.2.1 Calculation of the mass of the adsorbed binary PEC layers

The mass of the binary PEC layers adsorbed on the negatively charged SLB was calculated with the Sauerbrey equation, whereas the mass of the binary PEC layers adsorbed on the neutral SLB was calculated using Voigt based modeling (for which the chi² was below 2.1). Masses of the adsorbed binary PEC layers are summarized in Fig. 42. It shows that, in general, the mass of all PEC layers adsorbed on the negatively charged SLB was around 400 ng/cm² (which is in accordance with previous data[78]). It also shows that on the neutral SLB, the mass of binary PEC 1 layer was 1400 ng/cm², which is more than three times the value obtained in a previous study.[78]

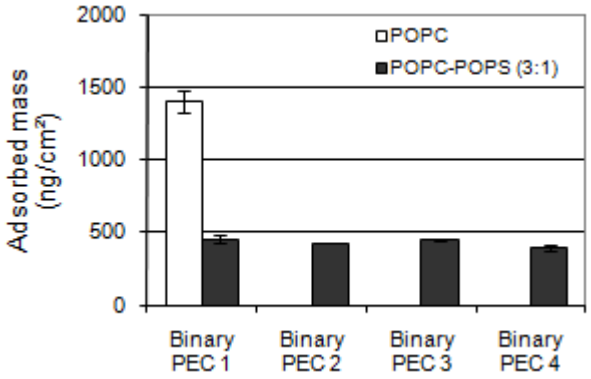

Fig. 42
Mass of the adsorbed PEC layers calculated using Sauerbrey equation for the layers adsorbed on POPC-POPS, and using Voigt-based modeling for the layers adsorbed on POPC

For the binary PEC 1 layer made on negatively charged SLB, we tried to determine the contribution of water with the reflectometry setup (data not shown). However, the result is not reliable because the QCM-D data measured in parallel did not reproduce previous data.[78]

XIII.3 Interaction between ternary PECs and SLBs

Fig. 43 shows the differences in adsorption profile, on a negatively charged SLB, between binary and ternary PECs. The ternary PECs, as opposed to binary PECs, yielded a transient peak in the frequency shift curve. The adsorption profile of the latter PECs is similar to previous data.[78] The transient peak was shorter and more important for ternary PEC 2 than for ternary PEC 1.

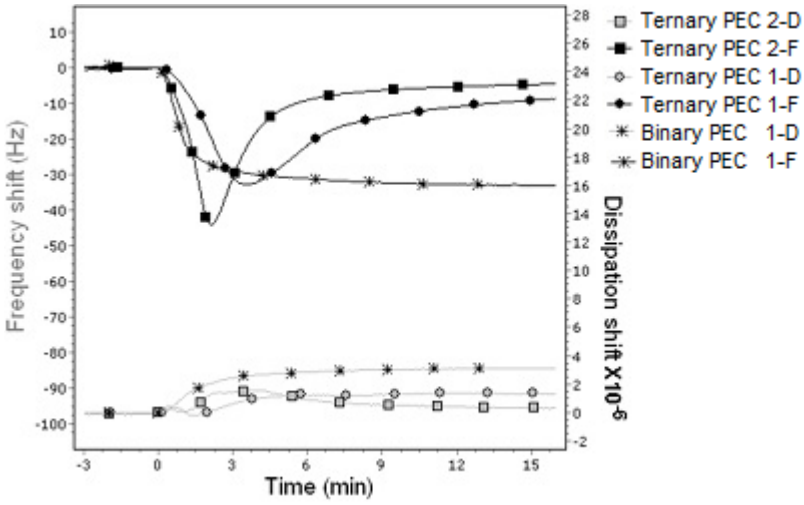

Fig. 43
Frequency and dissipation shifts (for the 9th overtone) during adsorption of binary PEC 1 and ternary PEC 1 and 2 on a negatively charged SLB made of POPC-POPS (3:1).

The frequency shift at equilibrium is much smaller for ternary PECs than for binary PECs (see Fig. 44). Note that the dissipation shift is rather low for all 3 PECs. For the 3 types of PEC, there was no spreading between measurements performed at different overtones.

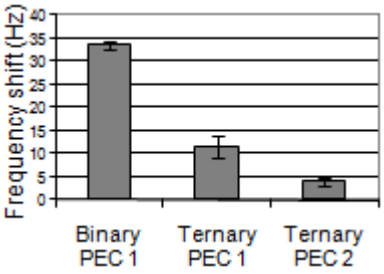

Fig. 44
Average and standard deviation of the frequency shift for the 9th overtone at equilibrium (based on 2 to 4 measurements)

Fig. 45 shows the differences in desorption profile, on a negatively charged SLB, between ternary and binary PECs at the rinsing step. Binary PECs presented a very low degree of reversibility. Ternary PEC 1 adsorbed completely irreversibly to the SLB. For ternary PEC 2, a rinsing step induced a low decrease in frequency, and a low increase in dissipation, indicating a mass uptake.

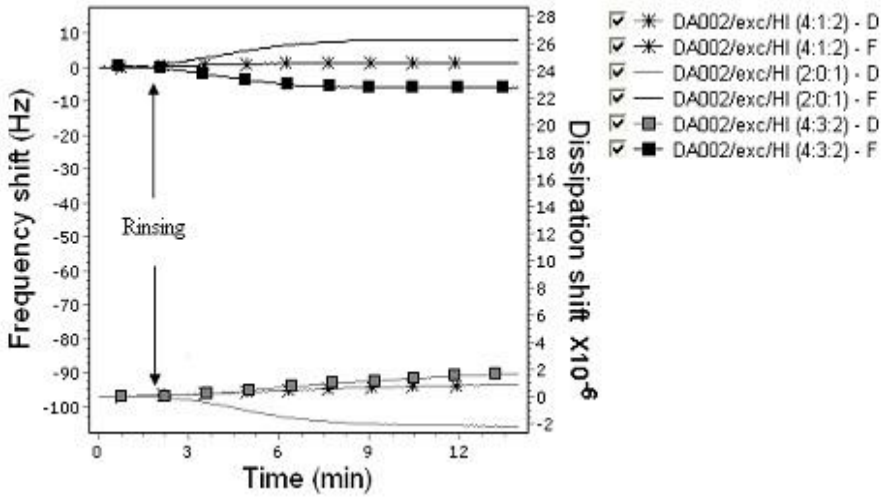

Fig. 45
Desorption profile of NPs with and without excipient at the 9th overtone on a negatively charged SLB.

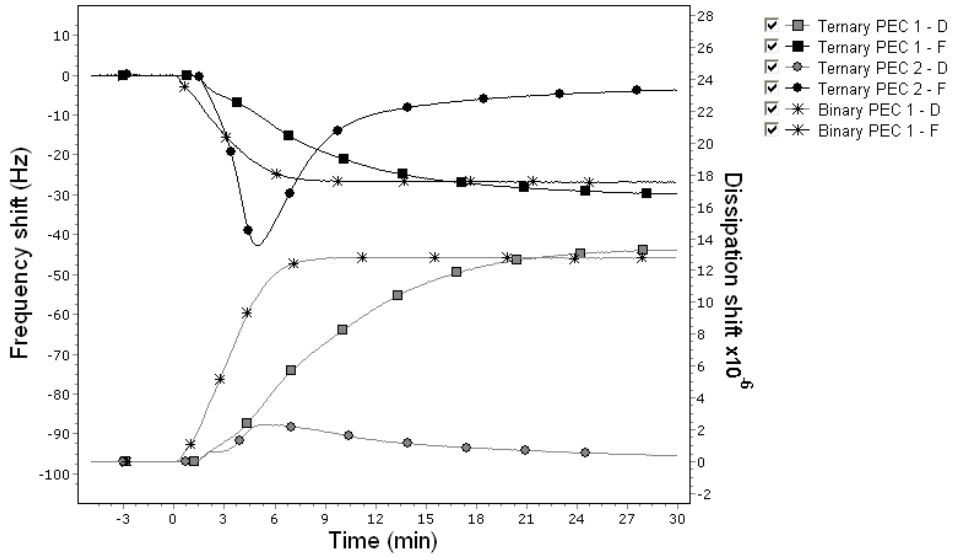

Fig. 46
Frequency and dissipation shifts (for the 9th overtone) during adsorption of ternary PEC 1 and 2, and of binary PEC 1 on a neutral SLB made of POPC

Fig. 46 shows that on the neutral SLB, only the ternary PEC 2 presents the same adsorption profile as on the negatively charged SLB. Ternary PEC 1 and binary PEC 1 did not show any transient peak, and

yielded much higher dissipation and frequency shifts, indicating the formation of a thick and viscoelastic layer.

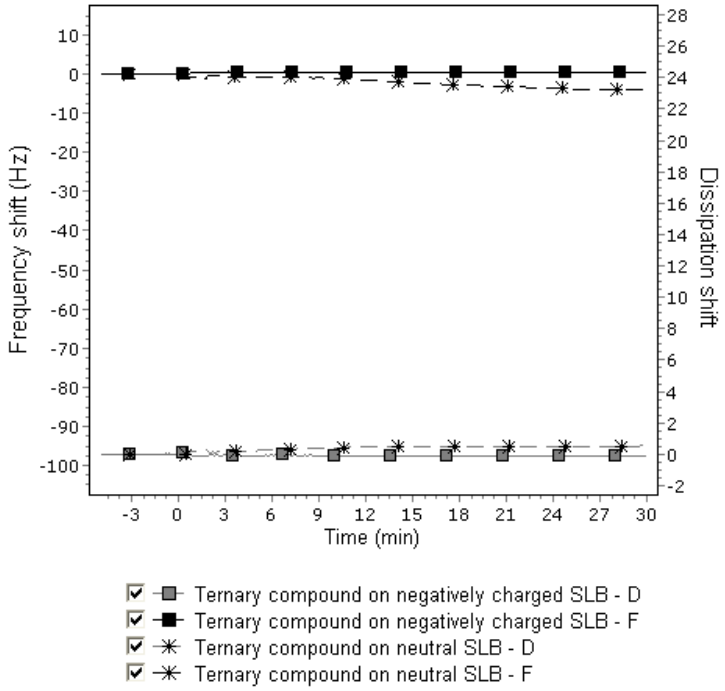

Fig. 47
Frequency and dissipation shifts (for the 9th overtone) during adsorption of the ternary compound on both neutral and negatively charged SLBs

The adsorption profile of the ternary compound on both neutral and negatively charged SLBs is plotted on Fig. 47. It shows that there is no significant interaction between the ternary compound and both types of SLB.

Fig. 48 shows the adsorption profile of the controls of PEC 1 and 2 containing no HI. One can see that they both presented a transient peak, indicating that it is the ternary compound that is responsible for this peak.

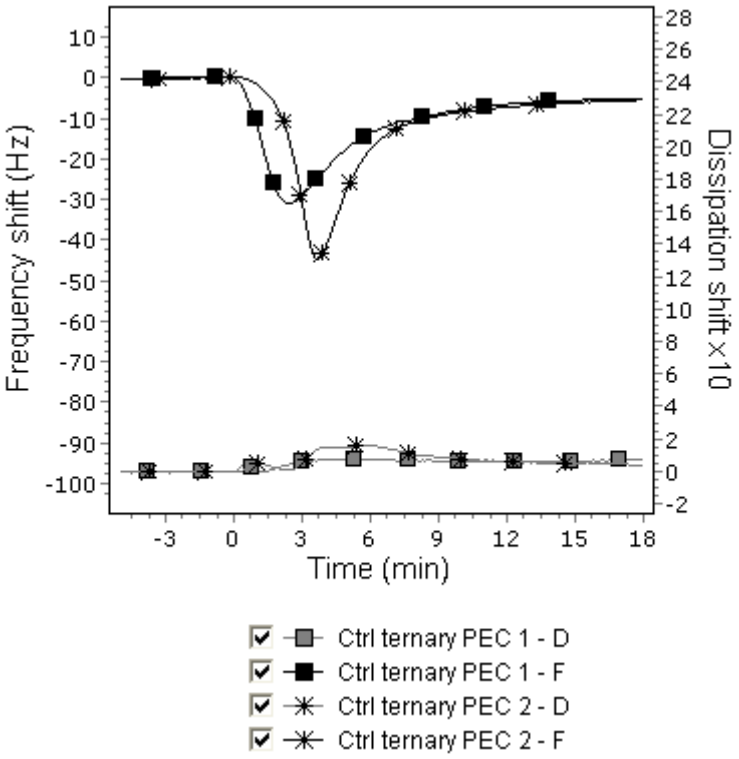

Fig. 48
Frequency and dissipation shifts (for the 9th overtone) during adsorption of Ctrl ternary PEC 1 and 2 on negatively charged SLB

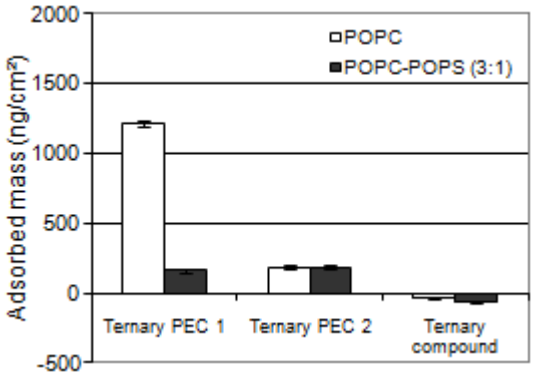

Fig. 49
Mass of the adsorbed ternary PEC 1 and 2 layers calculated using Sauerbrey equation for the layers adsorbed on POPC-POPS, and using Voigt-based modeling for the layers adsorbed on neutral SLB

Table 6 summarizes all frequency and dissipation shift values between equilibrium and rinsing step for the ternary PEC 1 and 2, for the controls of the latter (controls containing no HI), and for the ternary compound adsorbed on both types of SLB.

Table 6
QCM-D shifts for the 9th overtone upon rinsing after ternary PEC 1 and 2, and ternary compound adsorption

	POPC		**POPC-POPS (3:1)**	
	Frequency shift	**Dissipation shift**	**Frequency shift**	**Dissipation shift**
Ternary PEC 1	7.8±5.6	-4.3±3	2±2.3	0±0.8
Ternary PEC 2	-8.5±0.6	1.7±0.6	-7.5±0.9	1.5±0.5
Ctrl ternary PEC 1	-0.8±1.8	1.4±0.2	-2.8±0.4	1.8±0.4
Ctrl ternary PEC 2	-9±0.7	1.9±0.2	-6.8±1	1.5±0
Ternary compound	1.8±2.5	-0.2±0.2	6±0	-0.3±0

XIVElectrochemical impedance spectroscopy

Due to some problems in the experimental set up, the experiment could not be performed in good conditions and the data are not exploitable. Nevertheless, it would be very interesting to perform this experiment in a further work.

XV Discussion

XV.1 Quality assessment of the solutions

DLS and NTA are two techniques used in this work to measure the size of lipid vesicles, proteins, polycations and PECs in solution or suspension. Both techniques measure the Brownian motion of particles which is related to particle size through the Stokes-Einstein equation (Eq. 2). Based on the different ways of following light scattering, these two granulometric analyses are complementary and can provide different results. Herein, a good correlation was most of the time obtained between the two techniques (see for example results obtained for binary PEC in Table 4). However sometimes differences between the two techniques were pointed out (see for example results for LYSO in paragraph XV.1.1.1 below).

In NTA, individual particle positional changes are tracked in two dimensions, from which the particle diffusion can be deduced. Knowing the diffusion coefficient (D), the particle hydrodynamic diameter can be determined. NTA is an accurate method for sizing both monodisperse and polydisperse samples. The presence of a few large particles in a sample mainly constituted of particles of distinctly smaller size has little impact on NTA sizing accuracy. In contrast, in DLS the particles cannot be visualized individually. Instead it analyses the fluctuation of the intensity of the scattered light as a function of time. A mean size value of the hydrodynamic diameter is calculated. The mean size value is biased towards the largest particles/contaminants present within a sample. It is thus only comparable with the results of other techniques, if the sample is monodisperse. For polydisperse samples having a polydispersity index over 0.5, the mean size value is not reliable and can therefore only be used to compare results with samples measured by the same technique. This explains for example why DLS and NTA data gave different size values for the ternary PEC 2.[79] NTA yielded a mean size value of about 230 nm for those PECs, while DLS yielded the following values: mean diameter = 633 nm, PdI = 0.623.

XV.1.1 Protein solutions

XV.1.1.1 Lysozyme

DLS data showed LYSO as well solubilized, which is in correlation with what is found in the literature. [80-81] The main part of the solution consisted in monomers of hydrodynamic diameter < 2 nm, which is reasonable for a 14.7 kDa protein, and similar to previous results.[82] Traces of LYSO aggregates

[79] Filipe, Hawe et al., *Critical Evaluation of Nanoparticle Tracking Analysis (NTA) by NanoSight for the Measurement of Nanoparticles and Protein Aggregates*, Pharm. Res. (2010) **27:** 796-810
[80] Parmar and Muschol, *Lysozyme as diffusion tracer for measuring aqueous solution viscosity*, Journal of Colloid and Interface Science (2009) **339:** 243-248
[81] Ghalanbor, Korber et al., *Improved Lysozyme Stability and Release Properties of Poly(lactide-co-glycolide) Implants Prepared by Hot-Melt Extrusion*, Pharm. Res. (2010) **27:** 371-379
[82] Application note from Malvern Instrument http://www.malvern.com/common/downloads/campaign/MRK414-01.pdf

measuring 7.5 nm were also detected. However, according to NTA, the LYSO solution contained aggregates of sizes ranging from approximately 100 to 300 nm, independently of concentration. There is seemingly a contradiction between the results provided by the DLS and NTA techniques. If there were actually 200 nm aggregates in the LYSO solution, DLS should have detected them, especially because the measurement was performed during a long time (300 sec).

XV.1.1.2 Ovalbumin

We were confronted with a problem of OVA aggregation at pH 7.4. Our hypothesis is that denaturation of the protein is induced by exposing the protein to the air-water interface, as suggested in the literature. [83] This process is enhanced by agitation of the sample, which was also shown in similar experiments performed in Liège.[84] We finally investigated the influence of a time factor on the aggregation process, and concluded that aggregation is time dependant. Aggregates were already detected from the very beginning, and their amount increased as a function of time. Another previous study showed that by heating, OVA molecules denatured and aggregated into thin strands (such linear aggregates were also observed in this project, see Fig. 25 p. 30) or more dense particles (random aggregates) depending on the conditions used for the heat treatment (pH, ionic strength, and protein concentration). The study revealed that under conditions of high electrostatic repulsion (far from pI and at low ionic strength), denatured OVA mainly formed linear semi-flexible aggregates of approximately 5–12 nm. In addition, this study also stated that OVA is a protein especially sensible to surface denaturation and interfacial coagulation that is mainly responsible for the exceptional foaming properties of egg white.[85-86] In further work it would be interesting to investigate in more detail the influence of different modes of mixing as well as the influence of temperature, presence of O_2 in the buffer, salt concentration, and ionic strength on the aggregation process. Given that the problem of OVA aggregation could not be solved, the goal to form good quality protein solutions could not be reached and we had to choose another protein, HI, to prepare PEC solutions.

XV.1.1.3 Human Insulin

NTA data showed HI as well solubilized, although DLS measurement did not yield very good quality data. This can be explained by the property of HI to form amyloid fibrils.[87] The presence of such

---

Accessed the 28th of June, 2010.

[83] Lechevalier *et al.*, *Ovalbumin, ovotransferrin, lysozyme: Three model proteins for structural modifications at the air-water interface*, Journal of Agricultural and Food Chemistry (2003) **51:** 6354-6361

[84] Influence of agitation mode on OVA dissolution state, 2010, University of Liège

[85] Koseki *et al.*, *Irreversible thermal denaturation and formation of linear aggregates of ovalbumin*, Food Hydrocolloids (1989) **3:** 123-134

[86] Pouzot *et al., X-ray and light scattering study of the structure of large protein aggregates at neutral pH*, Food Hydrocolloids (2005) **19:** 231-238

[87] Rasmussen *et al.*, *The Molecular Chaperone alpha-Crystallin as an Excipient in an Insulin Formulation*, Pharm. Res. (2010) **27:** 1337-1347

structures could therefore increase the PdI of the solution, impairing the analysis of DLS data.

XV.1.2 Polycation and PEC solutions

Surprisingly, all binary and ternary PECs had a ZP of around +25 mV, although the ternary compound by itself had a charge of -43.2 mV. It is therefore surprising that we could not measure a clear difference of charge between the binary and ternary PECs. This can be explained by the fact that the ternary compound might be locked inside the NPs and be protected enough not to show at the surface of the particles. The fact that ternary PEC 2 was bigger and was a bit less positively charged than the ternary PEC 1 indicates that the ternary compound was not only free in the suspension of NPs, but was also coupled to the NPs. Obtaining positively charged PECs was very encouraging given that positively charged polymeric nanoparticles have been shown to promote transcytosis in epithelial cells.[88]

The main purpose of adopting polycations of different Mn is to verify if this molecular parameter could affect the in vitro stability of the resulting PECs and their biointeraction with model lipid membranes. From this point of view it is of interest to recall that the adoption of lower Mn polycations facilitates their body clearance and prevents potential cytotoxicity.[89]

XV.2 Quartz Crystal Microbalance with Dissipation monitoring analysis

Using the QCM-D technique, we studied how polycations and PECs interacted with 2 types of SLBs (neutral SLBs made of POPC, and negatively charged SLBs made of POPC-POPS (3:1)).

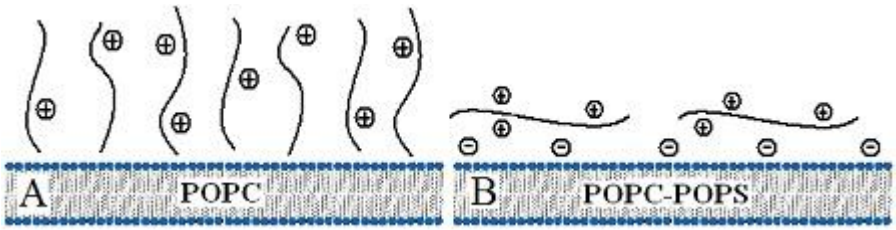

Fig. 50
On a neutral SLB the polymers form viscoelastic layers (A), and on the negatively charged SLB they form thin and rigid layers (B).

The adsorption profile of the four polycations on the neutral SLB was characterized by significantly different frequency and dissipation shifts for each different overtone, indicating that they formed a hydrated viscoelastic layer (see Fig. 50 A). On the contrary, their adsorption profile on the negatively charged SLB did not yield any dissipation shift at all, indicating that the polycations formed thin and rigid layers on that SLB. We interpreted these data as polycation collapse on the negatively charged SLB as soon as they come into contact with it. This is schematically represented in Fig. 50 B. In both cases, there was no change in frequency and dissipation shifts after rinsing, meaning that the four polycations irreversibly adsorbed to both types of SLB. The mass of the polycation layers formed on the neutral SLB was calculated using Voigt based modelling, whereas the mass of thin and rigid polycation layers formed

[88] O. Harush-Frenkel, E. Rozentur, S. Benita, Y. Altschuler, Surface charge of nanoparticles determines their endocytic and trancytotic pathway in polarized MDCK cells, Biomacromolecules, 9 (2008) 435-443.
[89] Fischer *et al.*, *In vitro cytotoxicity testing of polycations: influence of polymer structure on cell viability and hemolysis.*, Biomaterials (2003) **24:** 1121-1131

on the negatively charged SLB was calculated using the Sauerbrey equation.

Polycation 1, 2 and 4 formed a layer of about 700 to 800 ng/cm² on the neutral SLB (a reliable value could not be calculated for polycation 3 layer) and all 4 polycations formed a layer of about 400 ng/cm² on the negatively charged SLB. Likely, water content was higher in the softer layers formed on the neutral SLBs. These results emphasize that the electrostatic properties of the polycations are determinant for their interaction with SLBs.

The 4 polycations showed more negative ZP than the binary and ternary PECs (see Table 2) and also did not form aggregates, thus one can expect that they provide a completely different absorption profile. This is confirmed by the results, where the above polycations adsorbed in thinner layers with more rapid kinetics than the NPs did.

On the negatively charged SLB, all binary PECs but the one formed with the smaller polycation showed the same adsorption profile. The fact that the adsorption profile of binary PEC 4 was rather similar to the profile of polycation 4 indicates that polycation 4 was not properly complexed to HI through electrostatic interactions as it was supposed to be, and also as suggested by DLS and NTA data (see Table 3 p. 36). On the same type of SLB, there was a positive correlation between the dissipation shift and the Mn of the polycation used in binary PEC 1, 2 and 3. Thus, even though no difference as a function of Mn could be determined by size measurements, the binary PECs behaved quite differently when adsorbing to the SLBs, that is, as a function of Mn. The higher the Mn of the polycation used to make the binary PECs, the less the PEC layer was viscoelastic. A likely interpretation of these data is that for higher polycation Mn, the binary PECs collapse more easily when adsorbed to the SLB, owing to steric crowding. Note that all binary PEC layers adsorbed on the negatively charged SLB had about the same mass as the polycation layers adsorbed on the same SLB. These results suggest that there is a HI release during the adsorption of NPs on the SLB. Thus, NPs do not seem to keep their structure intact once they are adsorbed on the SLB, they rather seem

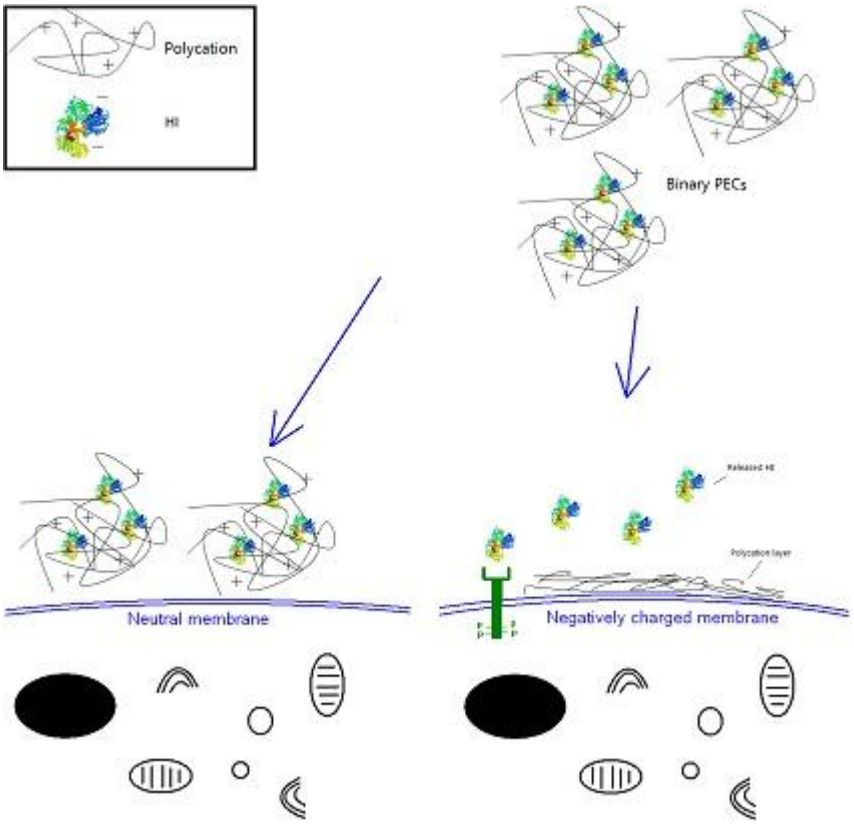

Fig. 51
Schematic drawing illustrating the interaction of binary PECs with neutral and negatively charged model lipid membranes

to collapse, and to release their HI content.

On the neutral SLB, only binary PEC 1 was investigated. It would be of interest to include the three other binary PECs in a further study. On that SLB, binary PEC 1 formed a thick and hydrated viscoelastic layer as described in a previous study.[78] That study contains more in-depth work, including the results of a complementary reflectometry measurement combined with QCM-D that has been done in order to determine the contribution of water to the mass of the binary PEC 1 hydrated layer on a neutral SLB. In the same study, m_{optic} was found to be 133 ng/cm², which is about one third of the acoustic mass measured with the QCM-D technique alone. The water content of this layer is then of about 70 % when $m_{acoustic}$ and m_{optic} are compared. The adsorption profile of binary PECs on neutral SLBs suggests that they remain relatively intact on the membrane, preventing the insulin from being released. Both binary PEC 1 and 2 formed a relatively stable layer on both types of SLB. However, binary PEC 3 layer was half reversible upon rinsing.

All binary PEC layers adsorbed on the negatively charged SLB corresponded to an adsorbed mass ranging between 400 and 450 ng/cm², which is in accordance with previous data[78]. However, on the neutral SLB, the mass of binary PEC 1 layer was 1400 ng/cm², which is more than 3 times the value obtained in the previous study cited above. The chi² value for this mass calculation was < 2.2.

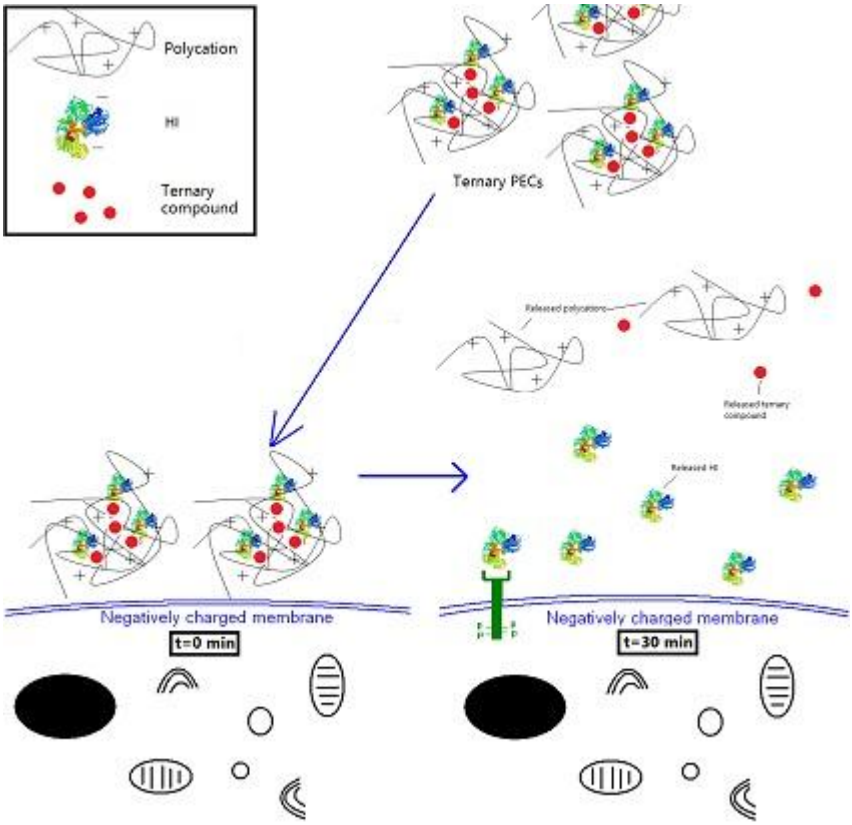

Fig. 52
Schematic drawing illustrating the interaction of ternary PECs with a negatively charged model lipid membrane, at t=0 and t=30 min.

The presence of a ternary compound in the ternary PEC formulation drastically affected the adsorption profile on the negatively charged SLB. A transient peak in the frequency shift curve appeared, suggesting that the ternary PECs first adsorbed intact on the membrane, forming a thick and hydrated layer, and, a few minutes later, collapsed, releasing the water molecules that were trapped in and in between the ternary PECs, and with them their HI content, after 30 minutes (see Fig. 52). On the neutral SLB, this change in adsorption profile is only noticed for ternary PEC 2. The presence of a transient peak in the frequency shift curve indicates a transient mass uptake. On the negatively charged SLB, the mass of

ternary PEC 1 and 2 layers was smaller than the mass of binary PEC 1 layers, although they all were thin and rigid.

We concluded that the ternary compound was the only one responsible for yielding a transient peak in the PEC adsorption profile.

XVIConclusion

This thesis reports on the interaction in real time of polymeric NPs, developed for diabetes treatment, with biomimetic model lipid membranes. For this interaction study we used two different model proteins (HI and OVA) and 4 polycations of different molecular weight. The study contains two main parts: a first one focusing on NP preparation and characterization, and a second one focusing on the study of the interaction between the NPs and two types of model lipid membranes.

First, by adopting polymers and procedures of the ULg**,** we successfully reproduced the preparation of those NPs either loaded with HI or chicken OVA. The formulation of OVA has highlighted interesting findings related to issues in its solubilisation; in particular, protein aggregation was easily induced over time and by agitation.

The sizes of the NPs were characterized with DLS and NTA. Those two techniques were compared in more detail, and, in general, a good agreement was obtained.

The second and main part of our work has been focused on the study of the in vitro interaction between the NPs loaded with HI and model lipid membranes, adopting the QCM-D technique. Two model lipid membranes differing in electrical charge were successfully formed. Our observations support that the four polycations irreversibly formed soft layers on neutral membranes, whereas they collapsed in the form of a stable, thin and rigid layer on negatively charged membranes. Although not really surprising, these data underscore the importance of electrostatic properties in the interaction of polycations with lipid membranes. On the negatively charged membrane, we found that the molecular weight of the free polycations did not affect their adsorption; whereas NPs formed relatively rigid layers having viscoelastic properties varying as a function of the molecular weight of the polycation used to prepare the NPs. The higher this molecular weight, the less soft the layer. On the neutral SLB, the NPs formed a thick and soft layer. Both binary PEC 1 and 2 (PECs synthesized with polycations having a Mn of 90000 and 40000 Da respectively) formed a relatively stable layer on negatively charged SLBs, whereas half of the binary PEC 3 layers was removed upon rinsing (PECs 3 were synthesized using a polycation having a Mn of 20000). The presence of a ternary compound in the formulation of the NPs drastically affected their adsorption profile on the negatively charged membrane, inducing a transient mass uptake. However, on the neutral membrane, only the adsorption profile of ternary PEC 2 seems to be affected by the ternary compound in the same way as it was affected when adsorbing on the negatively charged SLB. We found that the ternary compound was the only responsible for inducing a transient mass uptake.

XVII Acknowledgement

I am particularly grateful to my supervisor Mrs. Sofia Svedhem (assistant professor at the department of Applied Physics of Chalmers University of Technology, Sweden) for giving me the opportunity to realize this project in her group, and for her strong guidance and support all along the process of this master thesis. I thank Mr. Christian Grandfils (director of the CEIB, ULg) for his support, for the numerous suggestions and corrections he made on the manuscript, for everything he taught me, for the interest in biomaterials he awoke in me, for introducing me to Sofia Svedhem and for providing me with materials to work on. I thank Mr. Ricard Frost for teaching me the techniques used in this work and for his numerous helpful advices. I thank Chantal Sevrin and Natalia Kuznetsova for preparing the NPs studied in this work and for carrying out additional tests in vitro for the characterization of the OVA dissolution state. I thank the European Community and Novo for the gift of HI. I thank the whole group of Biological Physics of Chalmers for their advices and all kinds of help they gave me during this project. Finally, I would also like to thank Louis Pironт, my godfather, (Belgium) for boosting me in my knowledge of the English language.